Developing Intermolecular-Potential Models for Use with the SAFT-VR Mie Equation of State

Simon Dufal
Dept. of Chemical Engineering, Qatar Carbonates and Carbon Storage Research Centre, and Centre for Process Systems Engineering, Imperial College London SW7 2AZ, U.K.

Thomas Lafitte
Process Systems Enterprise Ltd., 26–28 Hammersmith Grove, London W6 7HA, U.K.

Amparo Galindo, George Jackson, and Andrew J. Haslam
Dept. of Chemical Engineering, Qatar Carbonates and Carbon Storage Research Centre, and Centre for Process Systems Engineering, Imperial College London SW7 2AZ, U.K.

A major advance in the statistical associating fluid theory (SAFT) for potentials of variable range (SAFT-VR) has recently been made with the incorporation of the Mie (generalized Lennard–Jones [LJ]) interaction between the segments comprising the molecules in the fluid (Lafitte et al. J. Chem. Phys. 2013;139:154504). The Mie potential offers greater versatility in allowing one to describe the softness/hardness of the repulsive interactions and the range of the attractions, which govern fine details of the fluid-phase equilibria and thermodynamic derivative properties of the system. In our current work, the SAFT-VR Mie equation of state is employed to develop models for a number of prototypical fluids, including some of direct relevance to the oil and gas industry: methane, carbon dioxide and other light gases, alkanes, alkyl benzenes, and perfluorinated compounds. A complication with the use of more-generic force fields such as the Mie potential is the additional number of parameters that have to be considered to specify the interactions between the model molecules, leading to a degree of degeneracy in the parameter space. A formal methodology to isolate intermolecular-potential models and assess the adequacy of the description of the thermodynamic properties in terms of the complex parameter space is developed. Fluid-phase equilibrium properties (the vapor pressure and saturated-liquid density) are chosen as the target properties in the refinement of the force fields; the predictive capability for other properties such as the enthalpy of vaporization, single-phase density, speed of sound, isobaric heat capacity, and Joule–Thomson coefficient, is appraised. It is found that an overall improvement of the representations of the thermophysical properties of the fluids is obtained using the more-generic Mie form of interaction; in all but the simplest of fluids, one finds that the LJ interaction is not the most appropriate. © 2015 The Authors AIChE Journal published by Wiley Periodicals, Inc. on behalf of American Institute of Chemical Engineers AIChE J, 61: 2891–2912, 2015
Keywords: equation of state, SAFT, phase equilibrium, complex fluids, second-derivative properties, parameter estimation

Introduction

Modelling the thermodynamics and fluid-phase equilibria of a system at the level of its constituent molecules is of central importance to chemical engineering and the applied physical sciences in general.[1] As pointed out by Redlich and Kwong[2] more than 60 years ago, it is desirable and convenient to have an algebraic method based on a suitable equation of state (EOS) for this purpose. The primary interest of Redlich and Kwong lay in the provision of an empirical relation for the description of (supercritical) gases (liquids are barely mentioned in their manuscript), and the nature of their modification of the pioneering cubic EOS of van der Waals[3,4] probably reflects this. With the passage of time the demands and interests of the engineering community have changed and evolved; Soave's modification[5] of the Redlich–Kwong EOS allowed for better performance in relation to describing vapor-liquid equilibrium (VLE), while Peng and Robinson's EOS[6] provided further improvement in relation to the hitherto poor descriptions of liquid densities with the Redlich–Kwong and Soave–Redlich–Kwong forms. Although a good description of fluid-phase equilibria in (p, V, T) space (where p is the pressure, V the volume, and T the temperature) probably remains the most important goal, there has subsequently been an ever increasing demand for methodologies that allow for greater predictive capabilities. This is true not only in terms of describing the complex phase behavior

Correspondence concerning this article should be addressed to A. J. Haslam at a.haslam@imperial.ac.uk.

exhibited by the multicomponent mixtures that are frequently of interest in modern engineering applications, but also in terms of providing a reliable and simultaneous description of other key-derived thermodynamic properties, such as heat capacities, speeds of sound, and Joule–Thomson coefficients; moreover, one may require a description of fluid-phase behavior in terms of other thermodynamic variables—for example, in the analysis of refrigeration or power cycles, a representation in either (T, S) or (p, H) space is more appropriate (where S is the entropy and H the enthalpy).

Although many further developments have been made with respect to the modelling of fluids and fluid mixtures with cubic EOSs and the current-day description is frequently excellent (see, e.g., the book of Kontogeorgis and Folas[7] for a more-detailed discussion), one is ultimately constrained by the simple nature of the underlying molecular model, which remains, at heart, van der Waals' attractive hard-sphere molecular model. The need to be able to predict or, at least, adequately describe the thermodynamic properties of fluids of greater molecular functionality in progressively more-complicated processes has, therefore, driven the development of increasingly sophisticated EOSs, based on more physically realistic molecular models. Among these are the molecular-based family of EOSs developed within the framework of the statistical associating fluid theory (SAFT),[8,9] the origins of which are firmly grounded in a formal statistical-mechanical treatment of continuum fluids.[10–15] To capture the essentials of asymmetries in molecular shape, molecules are modelled as chains of tangentially bonded spherical monomeric segments, which interact with each other through a prescribed potential. Moreover, the directional nature of intermolecular interactions between associating molecules can be accounted for by incorporating bonding sites on the molecular cores, mimicking the hydrogen bonding in fluids such as water or methanol.

Within the basic SAFT EOS methodology, one constructs the Helmholtz free energy of the fluid in the form of a perturbation theory starting with that of a reference monomeric fluid and adding contributions relating to the changes in free energy that would be brought about by, for example, irreversibly joining the monomers into chains, and by allowing molecules to associate with each other. The nature and expression of the different terms corresponding to these perturbative contributions are specific to each particular version of SAFT; indeed, it is these differences that characterize the various incarnations of the EOS. Among the more popular are the original SAFT,[8,9] Huang–Radosz (HR) SAFT[16] (sometimes referred to as CK-SAFT), simplified SAFT,[17] SAFT-Lennard-Jones (LJ),[18–21] SAFT-variable range (VR),[22,23] Soft-SAFT,[24,25] perturbed chain (PC)-SAFT,[26,27] and simplified PC-SAFT.[28] Group-contribution (GC) reformulations of SAFT have been developed by a number of groups[29–38]; these EOSs are continuum-fluid descendants of the seminal GC approach developed by Prausnitz and co-workers[39] within a quasi-chemical (lattice-based) framework for the activity coefficient of mixtures.[40] A discussion of the different versions of the SAFT EOS and the adequacy of representing the thermodynamics and fluid-phase equilibria of a broad variety of fluids and fluid mixtures with the methodology has now appeared in a number of excellent reviews.[7,41–45] It is clear from the chronology of this list that since the inception of

SAFT in the late 1980s, there has been continuous effort to improve the theory. An important recent development in this regard is the SAFT-VR Mie EOS,[46] and its GC offspring, SAFT-γ Mie[37].

The SAFT-VR Mie EOS[46] is an extension of the SAFT-VR[22,23] approach in which the underlying Barker and Henderson high-temperature perturbation expansion of the monomer free energy is incorporated to third order and, in particular, where the interactions between the monomeric segments are represented using Mie potentials,[47] that is, generalized LJ forms (with variable repulsive and attractive exponents). The refinements to the theory result in an EOS with substantially improved performance for the fluid properties as compared with SAFT-VR prior to its reformulation,[22,23,48–50] greatly enhancing the accuracy of the description of the near-critical region, while retaining the accurate modelling of second-derivative properties provided by the use of the Mie potential.[48–50] Combined with a novel treatment of the association contribution to the free energy,[51] these advances allow for a high-fidelity global representation of the thermodynamic properties and fluid-phase equilibria of associating molecules and their mixtures.

The Mie (λ_r-λ_a) potential for two spherical segments with centres separated by a distance r is given by

$$u^{\text{Mie}}(r) = \mathcal{C}(\lambda_r, \lambda_a)\varepsilon\left[\left(\frac{\sigma}{r}\right)^{\lambda_r} - \left(\frac{\sigma}{r}\right)^{\lambda_a}\right] \qquad (1)$$

Here, just as with the LJ (12-6) potential, σ is a size parameter representing the diameter of each spherical monomeric core, ε is an energetic parameter representing the depth of the potential well, λ_r and λ_a are the repulsive and attractive exponents, respectively, and the parameter $\mathcal{C}(\lambda_r, \lambda_a)$, which takes a value of 4 for the LJ potential, is defined as

$$\mathcal{C}(\lambda_r, \lambda_a) = \frac{\lambda_r}{\lambda_r - \lambda_a}\left(\frac{\lambda_r}{\lambda_a}\right)^{\frac{\lambda_a}{\lambda_r - \lambda_a}} \qquad (2)$$

such that the minimum of the potential well is at $-\varepsilon$. The two exponents of the Mie potential constitute two additional parameters as compared with the LJ potential (for which $\lambda_r = 12$ and $\lambda_a = 6$ are fixed) or one additional parameter as compared with the VR square-well (SW) potential (the interaction considered with the most frequently used formulation of SAFT-VR[22,23]). Although the fluid-phase behavior can usually be accurately described using a single fixed form of interaction, such as the LJ (12-6) potential, often one cannot obtain an accurate simultaneous description of the second-derivative properties, which are very sensitive to the precise nature of the repulsive interactions. Accordingly, the more-versatile form provided by the use of the Mie potential offers a distinct advantage over the use of the simple LJ model.

Conversely, the introduction of additional parameters raises issues relating to the possibility of model degeneracy: in parameterizing the force field for a given fluid, one may encounter a variety of different models that provide essentially equivalent performance. Issues of model degeneracy have already been recognized in the context of a SAFT description of associating fluids that require extra parameters to characterize the association interactions (see, e.g., Refs. 52,53). To best exploit the power of the SAFT-VR Mie EOS, it is necessary to assess the nature of any model

degeneracy and how it may be resolved, for example, with an awareness of the sensitivities of the property predictions to variations in the parameter values or by taking advantage of known physics to assign parameter values; the mathematically optimum model may not always provide the best physical model.[52] For our current work with SAFT-VR Mie, it is of particular importance to gain an understanding of the role of the repulsive range parameter, λ_r.

The success of SAFT in general, and the main source of the predictive capability it provides, is predicated on its solid foundation in statistical mechanics, which has allowed the incorporation of more of the molecular-level physics of the system than was previously possible (e.g., using cubic EOS). This is partly facilitated by the perturbative treatment of the free energy as a sum of individual contributions, which can be related to physical attributes such as molecular shape, or association interactions. The formulation of SAFT-VR for the Mie potential allows, in principle, even more detailed information relating to the physical interactions to be included. However, the danger is that one could, instead, lose contact with the physics by blindly manipulating any extra adjustable parameters that may have been introduced, thereby reducing the EOS simply to a very good correlative tool. In a separate publication,[51] this issue is examined in the context of associating fluids. The main purpose of our current contribution is to provide an understanding of the model-parameter space and how it relates to the performance of the SAFT-VR Mie EOS in describing thermodynamic properties of nonassociating fluids, thereby avoiding the trap of simply providing correlations, and exploiting the tremendous predictive capabilities of this new EOS.

Theory

The precise form developed for the SAFT-VR Mie EOS has been described in detail elsewhere[46]; here, we simply collect together the important expressions. The underlying molecular model of a nonassociating fluid is that of a chain of m bonded spherical segments, interacting via a Mie potential, as given in Eq. 1. The general SAFT EOS for a nonassociating fluid is expressed as

$$A = A^{\text{ideal}} + A^{\text{monomer}} + A^{\text{chain}} \tag{3}$$

where A represents the Helmholtz free energy. Conceptually, to build up the equation, one imagines first an ideal gas of particles. The second (monomer) term on the right-hand side of Eq. 3 represents the change in free energy brought about by introducing interactions between the monomeric segments (thereby conferring size on them), and the final (chain) term represents the change in free energy brought about by grouping the segments as molecular chains (each comprising m monomeric segments). This grouping confers shape on the model molecule, so that the ideal contribution to the free energy (the first term) is not simply that of the point-particle ideal gas; rather, it represents the free energy of an ideal gas of the molecules, represented by $A^{\text{ideal}} = N k_B T(\ln(\rho \Lambda^3) - 1)$, where N is the number of molecules, k_B is Boltzmann's constant, T is the absolute temperature, $\rho = N/V$ with V the volume, and Λ^3 is taken to represent the de Broglie volume, which incorporates all of the kinetic (translational, rotational, and vibrational) contributions to the partition function. (We do not consider associating molecules in this work, hence, no term appears to account for the free energy of association.)

Monomer term

As with the original formulation of SAFT-VR,[22] the Helmholtz free energy of the monomer fluid is expressed as a high-temperature perturbation expansion, but this time taken to third order[46]

$$\frac{A^{\text{monomer}}}{N k_B T} = m \left(a^{\text{HS}} + \frac{a_1}{k_B T} + \frac{a_2}{(k_B T)^2} + \frac{a_3}{(k_B T)^3} \right). \tag{4}$$

For pure components, the free energy of the reference hard-sphere (HS) system is obtained from the well-known Carnahan and Starling[54] EOS as

$$a^{\text{HS}} = \frac{4\eta - 3\eta^2}{(1-\eta)^2} \tag{5}$$

where $\eta = \rho_s \pi d^3 / 6$ is the packing fraction of the reference HS system, and $\rho_s = N_s/V$ is the segment density of the Mie fluid, with $N_s = Nm$, the total number of segments. The Barker and Henderson[55] effective HS diameter $d(T)$ has been introduced as

$$d(T) = \int_0^\sigma 1 - \exp\left(\frac{u^{\text{Mie}}(r)}{k_B T}\right) dr \tag{6}$$

to represent the repulsive reference system.

The first-order perturbation contribution of the SAFT-VR Mie EOS is given by

$$a_1 = \mathcal{C}(\lambda_r, \lambda_a) \left[x_0^{\lambda_a} \left(a_1^S(\eta; \lambda_a) + B(\eta; \lambda_a) \right) - x_0^{\lambda_r} \left(a_1^S(\eta; \lambda_r) + B(\eta; \lambda_r) \right) \right] \tag{7}$$

where $x_0 = \sigma/d$,

$$B(\eta; \lambda) = 12\eta\varepsilon \times \left(\frac{(1-\eta/2)}{(1-\eta)^3} \left(\frac{1-x_0^{3-\lambda}}{\lambda-3} \right) - \frac{9\eta(1+\eta)}{2(1-\eta)^3} J_\lambda(\lambda) \right) \tag{8}$$

and

$$J_\lambda(\lambda) = -\frac{x_0^{4-\lambda}(\lambda-3) - x_0^{3-\lambda}(\lambda-4) - 1}{(\lambda-3)(\lambda-4)} \tag{9}$$

for both $\lambda = \lambda_a$ and $\lambda = \lambda_r$. The term a_1^S appearing in Eq. 7 is the first-order perturbation term for a Sutherland fluid, which can be obtained as

$$a_1^S(\eta; \lambda) = -12\varepsilon\eta \left(\frac{1}{\lambda-3} \right) \frac{(1-\eta_{\text{eff}}(\eta; \lambda)/2)}{(1-\eta_{\text{eff}}(\eta; \lambda))^3} \tag{10}$$

with

$$\eta_{\text{eff}}(\eta; \lambda) = c_1(\lambda)\eta + c_2(\lambda)\eta^2 + c_3(\lambda)\eta^3 + c_4(\lambda)\eta^4 \tag{11}$$

where the coefficients c_1, c_2, c_3, and c_4 are given in Eq. 41 of Ref. 46.

The second perturbation term is given by

$$a_2 = \frac{K^{\text{HS}}}{2}(1+\chi)\varepsilon\mathcal{C}^2(\lambda_r, \lambda_a)[x_0^{2\lambda_a}(a_1^S(\eta; 2\lambda_a) + B(\eta; 2\lambda_a))$$
$$- 2x_0^{\lambda_a + \lambda_r}(a_1^S(\eta; \lambda_a + \lambda_r) + B(\eta; \lambda_a + \lambda_r))$$
$$+ x_0^{2\lambda_r}(a_1^S(\eta; 2\lambda_r) + B(\eta; 2\lambda_r))] \tag{12}$$

where K^{HS} is the isothermal compressibility of the hard-

sphere reference fluid, obtained from the Carnahan and Starling[54] expression for the compressibility factor as

$$K^{HS} = \frac{(1-\eta)^4}{1+4\eta+4\eta^2-4\eta^3+\eta^4} \quad (13)$$

and

$$\chi = f_1(\alpha)\eta x_0^3 + f_2(\alpha)\left(\eta x_0^3\right)^5 + f_3(\alpha)\left(\eta x_0^3\right)^8. \quad (14)$$

The functions $f_i(\alpha)$ characterizing the correction factor χ are obtained as

$$f_i(\alpha) = \frac{\sum_{n=0}^{3} \phi_{i,n}\alpha^n}{1+\sum_{n=4}^{6} \phi_{i,n}\alpha^{n-3}} \quad (15)$$

where the dimensionless van der Waals-like integrated attractive energy α is defined as

$$\alpha = \mathcal{C}(\lambda_r, \lambda_a)\left(\frac{1}{\lambda_a - 3} - \frac{1}{\lambda_r - 3}\right) \quad (16)$$

and the coefficients $\phi_{i,n}$ are taken from Table II of Ref. 46.

The third perturbation term is also expressed in terms of the functions $f_i(\alpha)$ as

$$a_3 = -\varepsilon^3 f_4(\alpha)\eta x_0^3 \exp\left(f_5(\alpha)\eta x_0^3 + f_6(\alpha)\eta^2 x_0^6\right). \quad (17)$$

Chain term

The chain term is expressed in the usual SAFT form as

$$\frac{A^{chain}}{Nk_B T} = -(m-1)\ln g^{Mie}(\sigma). \quad (18)$$

The radial distribution function (RDF) of the Mie fluid at contact is obtained as a second-order expansion:

$$g^{Mie}(\sigma) = g_d^{HS}(\sigma)\exp\left[\frac{g_1(\sigma)}{g_d^{HS}(\sigma)}\frac{\varepsilon}{k_B T} + \frac{g_2(\sigma)}{g_d^{HS}(\sigma)}\frac{\varepsilon^2}{(k_B T)^2}\right]. \quad (19)$$

The RDF of the reference fluid comprising HSs of diameter d evaluated at σ is calculated from

$$g_d^{HS}(\sigma) = \exp\left[k_0 + k_1 x_0 + k_2 x_0^2 + k_3 x_0^3\right] \quad (20)$$

wherein the coefficients k_i are given by

$$k_0 = -\ln(1-\eta) + \frac{42\eta-39\eta^2+9\eta^3-2\eta^4}{6(1-\eta)^3} \quad (21)$$

$$k_1 = \frac{-12\eta+6\eta^2+\eta^4}{2(1-\eta)^3} \quad (22)$$

$$k_2 = \frac{-3\eta^2}{8(1-\eta)^2} \quad (23)$$

and

$$k_3 = \frac{3\eta+3\eta^2-\eta^4}{6(1-\eta)^3}. \quad (24)$$

The first-order perturbation term in Eq. 19 is obtained from

$$g_1(\sigma) = \frac{1}{2\pi\varepsilon d^3}\left[3\frac{\partial a_1}{\partial \rho_s} - \mathcal{C}(\lambda_r, \lambda_a)\lambda_a x_0^{\lambda_a}\frac{a_1^S(\eta;\lambda_a)+B(\eta;\lambda_a)}{\rho_s}\right.$$
$$\left. + \mathcal{C}(\lambda_r, \lambda_a)\lambda_r x_0^{\lambda_r}\frac{a_1^S(\eta;\lambda_r)+B(\eta;\lambda_r)}{\rho_s}\right] \quad (25)$$

and the second-order perturbation term from

$$g_2(\sigma) = \frac{1+\gamma_c}{2\pi\varepsilon^2 d^3}\left\{3\frac{\partial a_2/(1+\chi)}{\partial \rho_s} - \varepsilon K_{HS}\mathcal{C}^2(\lambda_r, \lambda_a)\right.$$
$$\times\left(\lambda_r x_0^{2\lambda_r}\frac{a_1^S(\eta;2\lambda_r)+B(\eta;2\lambda_r)}{\rho_s}\right.$$
$$-(\lambda_r+\lambda_a)x_0^{\lambda_r+\lambda_a}\frac{a_1^S(\eta;\lambda_r+\lambda_a)+B(\eta;\lambda_r+\lambda_a)}{\rho_s}$$
$$\left.\left. + \lambda_a x_0^{2\lambda_a}\frac{a_1^S(\eta;2\lambda_a)+B(\eta;2\lambda_a)}{\rho_s}\right)\right\} \quad (26)$$

where

$$\gamma_c = \phi_{7,0}\left(-\tanh\left(\phi_{7,1}(\phi_{7,2}-\alpha)\right)+1\right)\eta x_0^3$$
$$\times\left(\exp\left(\frac{\varepsilon}{k_B T}\right)-1\right)\exp\left(\phi_{7,3}\eta x_0^3 + \phi_{7,4}\eta^2 x_0^6\right). \quad (27)$$

The coefficients $\phi_{7,i}$ ($i = 0, 3,$ and 4) are available from Table II of Ref. 46.

Fluid-phase coexistence requires the conditions of thermal, mechanical, and chemical equilibrium, which can be solved for a pure component by ensuring that the temperature, pressure, and chemical potential are equal in each phase. Having specified the explicit form of the Helmholtz free energy, the pressure $p = -(\partial A/\partial V)_{N,T}$, chemical potential $\mu = (\partial A/\partial N)_{V,T}$, and other thermodynamic properties can be obtained algebraically from the standard thermodynamic relations.[56] As well as the fluid-phase equilibrium properties, in our current work, we assess the adequacy of the SAFT-VR Mie EOS in describing second-order derivative properties[56] including the isobaric heat capacity c_p, the speed of sound u, and the Joule–Thomson coefficient μ_{JT}.

Method

In the SAFT-VR Mie approach, one represents molecules as bonded spherical segments interacting through Mie pair potentials so that the parameters defining the model of a molecule (in the case of nonassociating fluids) comprise the number of segments m forming the model molecule, and the parameters of the Mie potential, σ, ε, λ_r, and λ_a. As is customary in the development of models for use with an EOS, the values of these parameters are estimated using experimental pure-component information; one adjusts the values to minimize the difference between the experimental and calculated properties. We choose to minimize an objective function of the following form:

$$F_{obj} = \sum_X \left(\frac{\omega_X}{n_X}\sum_{k=1}^{n_X}\left[\frac{X_k^{exp}-X_k^{calc}}{X_k^{exp}}\right]^2\right) \quad (28)$$

where n_X is the number of datapoints relating to a given property X, ω_X is the weight assigned to property X, and k is a specific datapoint; a Levenberg–Marquardt algorithm is used[57,58] for the minimization procedure. A convenient measure of the quality of the description with the model is the

percentage absolute average deviation (%AAD) from experimental values of a property, calculated as

$$\%\text{AAD}(X) = \frac{100}{n_X} \sum_{k=1}^{n_X} \left| \frac{X_k^{\text{exp}} - X_k^{\text{calc}}}{X_k^{\text{exp}}} \right|. \qquad (29)$$

One can incorporate different properties in the objective function. Whereas parameter estimation for the previous formulation of SAFT-VR (using the SW potential) was mostly restricted to the description of vapor-liquid equilibria including the vapor pressure and saturated-liquid density—as is common practice for model development in relation also to other EOSs—the ability of SAFT-VR Mie to provide quantitative agreement for different second-derivative properties such as the speed of sound and heat capacity[46,48–50] allows one to include other properties in the objective function. A variation of the respective weights of the properties will result in different "optimal" estimated models, each tailored according to important features of the task at hand. One must choose not only the properties to include and their relative weights but, also, the range of experimental conditions (e.g., in temperature and pressure); this will also impact the %AADs and, thereby, the model highlighted as "optimal," so should be selected with care. (We note in passing that when using %AADs as a basis for comparison of different models, it is important that the experimental data sets against which the %AADs are calculated are identical; if they are not, the comparison can be somewhat misleading.)

In order to investigate the parameter space, we extend the method developed in Ref. 52 and used subsequently in Ref. 53; both these studies were carried out with the previous formulation of SAFT-VR using the SW potential, given by

$$u^{\text{SW}} = \begin{cases} +\infty & r < \sigma^{\text{SW}} \\ -\varepsilon^{\text{SW}} & \sigma^{\text{SW}} \leq r < \lambda^{\text{SW}}\sigma^{\text{SW}} \\ 0 & r \geq \lambda^{\text{SW}}\sigma^{\text{SW}} \end{cases} \qquad (30)$$

where σ^{SW}, ε^{SW}, and λ^{SW} represent the size, energy, and range parameters of the model. This method consists of performing multiple optimizations to obtain models for the same fluid with the same objective function, but using different fixed values for two of the parameters in each. Every point in the parameter-space plane formed by these two parameters then represents a model that is optimal in the remaining parameters, and different properties of the model, such as the %AAD or the objective function, can be easily represented using contour plots projected onto the plane defined by the two fixed parameters. In studies of water,[52] an almost identical representation of the properties is obtained with a number of different models, for broad intervals of the interaction energies; this degeneracy of parameters led to difficulty in identifying the best model. In the context of water models (of the type used in SAFT) one of the most useful characteristics is the ratio of the dispersion and associating contributions; accordingly, the plane selected was that defined by the parameters representing the depths of the dispersion and association energies.[52] Conversely, dos Ramos et al.[53] considered different pairs of parameters, (m, λ^{SW}) and $(\sigma^{\text{SW}}, \lambda^{\text{SW}})$ for nonassociating molecules, and $(\varepsilon^{\text{HB}}, \lambda^{\text{SW}})$ for water, that is, representing a geometric and an energetic parameter: by fixing one parameter (in this case m) to a specific value a more clearly identifiable optimal model can be obtained. In our current work, we extend the idea further, considering initially all 10 of the

parameter-space planes defined by pairs of the five model parameters of the molecules formed from Mie segments (m, ε, σ, λ_a, and λ_r). A case study in the development of such models is first undertaken for a carefully chosen fluid, to examine in detail the nature of the parameter space. Based on understanding gained in this case study, a subset of these planes is then chosen for the subsequent development of models of other fluids.

It remains only to select a suitable fluid on which to base the case study. The fluid selected for this purpose should be one for which the SAFT-VR Mie EOS is expected to provide an accurate representation of the thermophysical properties, for which one can readily judge the physical significance (or lack thereof) of the model parameters, and for which reliable experimental data are plentiful. Methane is an ideal candidate for such a study, fulfilling all of these criteria. A model for methane has already been developed for use with the SAFT-VR Mie EOS which provides an excellent description of the VLE and single-phase properties.[46] The leading multipole moment of methane is the octupole; this is not expected to make a significant contribution to the intermolecular interactions, which are, therefore, expected to be of London-dispersion form, with $\lambda_a = 6$. The spherical-top symmetry of methane suggests that it can be treated as a near-spherical molecule so that $m \sim 1$ is expected; moreover, from quantum-mechanical calculations,[59] one expects an average molecular diameter $\sigma \sim 3.7$Å. Although physically sensible values for the remaining two parameters, ε and λ_r, cannot so readily be anticipated, one would intuitively expect ε/k_B to be of the order of a few hundred kelvin. The ability to return physically reasonable parameter values close to these will provide a good test of our parameter estimation procedure based on the individual planes, and a means for the selection of the appropriate plane or planes to use in subsequent model development.

Results

Developing models for methane: detailed investigation of the parameter space

Estimations of model parameters for methane are performed for the 10 different planes defined by pairs taken from the five model parameters: (ε, λ_r); (ε, λ_a); (λ_a, λ_r); (m, λ_r); (m, λ_a); (σ, λ_r); (σ, λ_a); (ε, m); (ε, σ); and (m, σ). The values of the objective function (Eq. 28) and %AAD (Eq. 29) are calculated using the correlated experimental data from the National Institute of Standards and Technology (NIST)[60]; different properties are chosen, including saturation properties (the vapor pressure and saturated-liquid density), the single-phase density, and the speed of sound (21 points are taken in the range $T = 95 - 185$ K for each of the VLE properties, and 30 points for each of the single-phase properties, at conditions ranging from $T = 100 - 190$ K and $p = 10 - 50$ MPa).

The objective-function landscape for the SAFT-VR Mie models of methane in relation to each of the planes is characterized by two distinct valleys, the minima of which correspond to the same two models irrespective of the plane. A selection of contour plots relating to these are provided for illustration in Figure 1; for this examination, the objective function comprised the vapor pressure and saturated-liquid density (with equal weights, $\omega = 1$). Immediately it is apparent that one of these valleys corresponds to physically more-realisitic models, with $\sigma \sim 3.7$Å and $m \sim 1$, while the

Figure 1. Behavior of an objective function (Eq. 28) comprising the saturation properties of methane including the vapor pressure and saturated-liquid density (with equal weights, $\omega = 1$) obtained with the SAFT-VR Mie EOS[46] for planes of pairs of intermolecular parameters: (a) the (ε, λ_r) plane; (b) the (λ_a, λ_r) plane; (c) the (m, λ_a) plane; (d) the (m, λ_r) plane; (e) the (σ, λ_a) plane; and (f) the (σ, λ_r) plane.

Contours are projected onto each plane; blue areas correspond to lower and red to higher values of the objective function [the quantification of the color scale, common to each frame, is indicated in (b)]. Two distinct valleys are present no matter the plane considered, with minima corresponding to the same models. [Color figure can be viewed in the online issue, which is available at wileyonlinelibrary.com.]
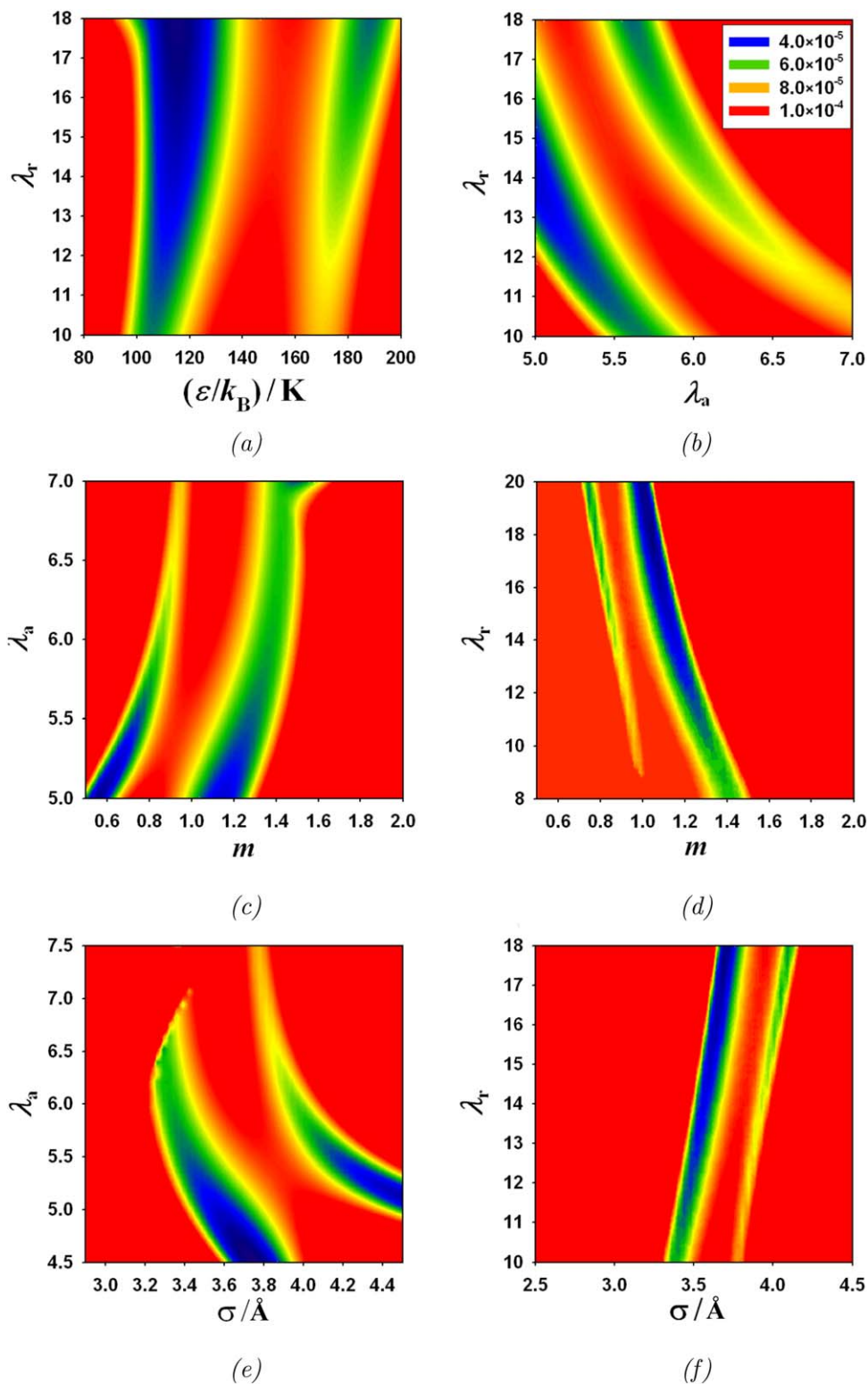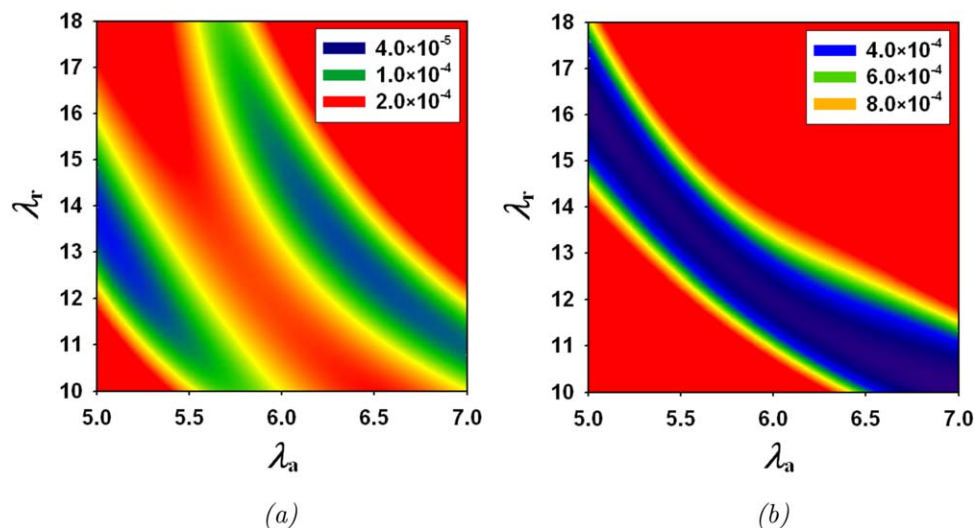
Figure 2. Behavior of an objective function (Eq. 28) comprising the saturation and single phase properties of methane including the vapor pressure, saturated-liquid density, single-phase liquid density (each with weight $\omega = 1$), and speed of sound (with weight $\omega = 0.25$) obtained with the SAFT-VR Mie EOS[46] for the plane comprising the pair of Mie exponents (λ_a, λ_r); in (a) m is estimated freely, while in (b) $m = 1$ is prescribed.

Blue areas correspond to lower and red to higher values of the objective function; note that the color scales are chosen to provide the best contrast in each figure, whereby that in (b) differs from that in (a). [Color figure can be viewed in the online issue, which is available at wileyonlinelibrary.com.]

models in the other valley feature $\sigma > 4\text{Å}$ and $m < 0.8$; the latter, in particular, is nonphysical, since $m = 1$ (representing a single spherical segment) is a lower bound. Models in both valleys are characterized by values of $\lambda_a \sim 5$; reassuringly, this is close to the London-dispersion value, although it is notable that the deviation, while small, leads to values lower and not higher than six.

In each of these estimations, two parameters defining the individual plane are fixed while the remaining three are free to adopt whatever values provide the optimal model. However, in certain circumstances, the values of one or more of these parameters may be determined by physical constraints. For example, as already noted, to be commensurate with the approximate spherical symmetry of the methane molecule, $m = 1$ is appropriate. Having already observed that only one of the two valleys observed in each of the contour plots given in Figure 1 corresponds to $m \sim 1$, one would expect that assigning $m = 1$ would have the effect of removing one of the valleys, thereby simplifying the objective-function landscape.

In Figure 2, we provide a comparison between the SAFT-VR Mie models obtained in the case where m is free (Figure 2a) and the case where $m = 1$ is assigned (Figure 2b); the behavior of an expanded objective function comprising the vapor pressure, saturated liquid density, single-phase compressed-liquid density (each given weight $\omega = 1$ in Eq. 28), and the speed of sound (with weight $\omega = 0.25$) is projected onto the (λ_a, λ_r) plane. From a comparison of Figures 2a, b, it is evident that the objective-function landscape is altered by fixing m, and that the resulting high-quality models are restricted to a narrower portion of parameter space, in accordance with the findings of dos Ramos et al.[53] Moreover, assigning $m = 1$ indeed simplifies the objective-function landscape, removing one of the valleys. Qualitatively similar results are obtained by fixing the attractive exponent to the London value of $\lambda_a = 6$ though, of course, one projects the landscape onto a different plane of parameter space.

In passing, it is interesting to note from Figure 2a that the inclusion of extra properties (namely, the single-phase density and speed of sound) in the objective function has resulted in one of the two valleys from the equivalent plot in Figure 1b being shifted to higher values of λ_a, and that it now encompasses the London-dispersion value $\lambda_a = 6$.

For our study of the SAFT-VR Mie models of methane, we had in advance some sense of physically sensible parameter values, specifically $m = 1$ and $\lambda_a = 6$, however, this will certainly not be the case for all molecules, and more-general strategies for judging parameters are desirable. One such strategy would be to consider a representation of the molecules at the van der Waals' level, that is, in terms of the corresponding excluded volume and integrated attractive energy. It is not straightforward to determine the excluded volumes for the chains of segments that comprise models of molecules in SAFT, however, the volume occupied by the molecules is proportional to $\mathcal{V} = m\sigma^3$, whereby $\mathcal{V}$ is a more convenient measure to consider. In Figure 3, the values for $\mathcal{V}$ of methane models obtained in the examination of the (λ_a, λ_r) plane (in which m is not constrained) are illustrated; see also Figure 1b for the objective-function landscape corresponding to this examination. The variation in $\mathcal{V}$ is less than 10% across the whole plane, demonstrating that no matter which Mie potential is used, the volume of all models of methane enabling a good description of the properties must lie within a narrow range. Moreover, by comparing this figure with Figure 1b, within the valley corresponding to the best models, it can be seen that the variation of $\mathcal{V}$ is less still. (The same conclusions can be drawn from an analogous inspection of molecular volumes corresponding to the landscape illustrated in Figure 2a, relating to the objective function incorporating the single-phase liquid density and speed of sound for methane in addition to the saturation properties.)

The integrated van der Waals attractive energy for a chain of m segments can be characterized in terms of the parameter α introduced earlier in Eq. 16 as
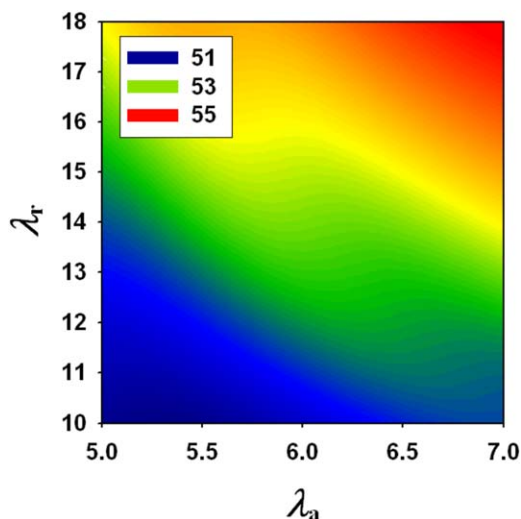
Figure 3. Molecular volume of the SAFT-VR Mie model for methane as characterized by the parameter $\mathcal{V}=m\sigma^3$ (in units of $\mathrm{Å}^3$) corresponding to optimizations in the plane comprising the pair of Mie exponents (λ_a, λ_r).

Blue areas correspond to lower and red areas to higher volumes. The parameter estimations are carried out using an objective function (see Eq. 28) comprising the vapor pressure and saturated-liquid density, each with equal weight ($\omega = 1$). (The objective-function landscape corresponding to this plane is given in Figure 1b.) [Color figure can be viewed in the online issue, which is available at wileyonlinelibrary.com.]

that of the triple-point, is shown for the case of spherical models; its use to develop coarse-grained potentials is highlighted in that work.

As a final observation in relation to Figure 4, one can discern from a comparison with Figure 1b (in which the same objective function is used) that the models providing the very best description of the heat capacity are not those that give the best description of saturation properties. Importantly, however, there is some overlap in which both sets of properties are well described—this means that although one should tailor one's model if a property such as c_p is of the utmost importance, one clearly does not need to sacrifice a good representation of the vapor-liquid equilibria, nor vice versa.

At this point, it is helpful to collect the insights gained in the foregoing discussion. In particular:

- As expected, the SAFT-VR Mie EOS provides for an excellent overall description of many of the thermodynamic properties of methane.
- Allowing the two exponents, λ_r and λ_a, to vary freely leads to an increasing complexity of the optimization.
- An appropriate form of the Mie potential can be identified by considering the integrated energy parameter α, as illustrated in Figure 4.
- The objective function surface is very sensitive to the properties included, together with their respective weights, and to whether or not any parameters are fixed. As a consequence, the objective function surface

$$E_{\mathrm{int}} = m^2\sigma^3\varepsilon\alpha. \qquad (31)$$

The energy E_{int} spans over a wider range than $\mathcal{V}$ (~100%), mainly because α varies almost threefold in this region. The importance of α can be seen in Figure 4, wherein contours representing the %AAD of the experimental isobaric heat capacity c_p from the corresponding values calculated with the SAFT-VR Mie EOS are plotted in the (λ_a, λ_r) plane along with contours representing constant values of α. The close correspondence between the two sets of contours indicates that models providing equivalent representations of the heat capacity correspond to similar values of α. In fact, by comparison of the contours in Figure 4 with those in Figures 1a and 2a, b, it is clear that the curvatures of the lines of constant α also broadly follow the contours of the optimum-parameter-space landscape. Single-segment Mie fluids with the same value of α have been shown to be conformal,[61] even though Mie fluids with different values of one or both of the exponents λ_r and λ_a are not generally conformal. This suggests that one can use α to inform the selection of an appropriate form of the Mie potential to characterize a model; for example, should a parameter estimation return an otherwise excellent model that has an unphysical value of one or both of the exponents, it indicates that this model can be replaced by another more-physical model, without serious detriment to the description of c_p or, indeed to the performance of the model in general, provided it has the same value of α. In Ref. 61, a relation between α and the range of the fluid as described by the ratio of the critical-point temperature to

Figure 4. Behavior of the %AAD (Eq. 29) of the experimental isobaric heat capacity c_p of methane from the corresponding values calculated with the SAFT-VR Mie EOS[46] (blue areas correspond to lower and red to higher AAD values).

The dashed white curves correspond to contours of the integrated energetic parameter α. The close coincidence in the shapes of the two sets of contours demonstrates that models yielding similar heat capacities are characterized by similar values of α. [In the parameter estimation, the objective function (Eq. 28) comprised the vapor pressure and saturated-liquid density with equal weights ($\omega=1.0$).] [Color figure can be viewed in the online issue, which is available at wileyonlinelibrary.com.]
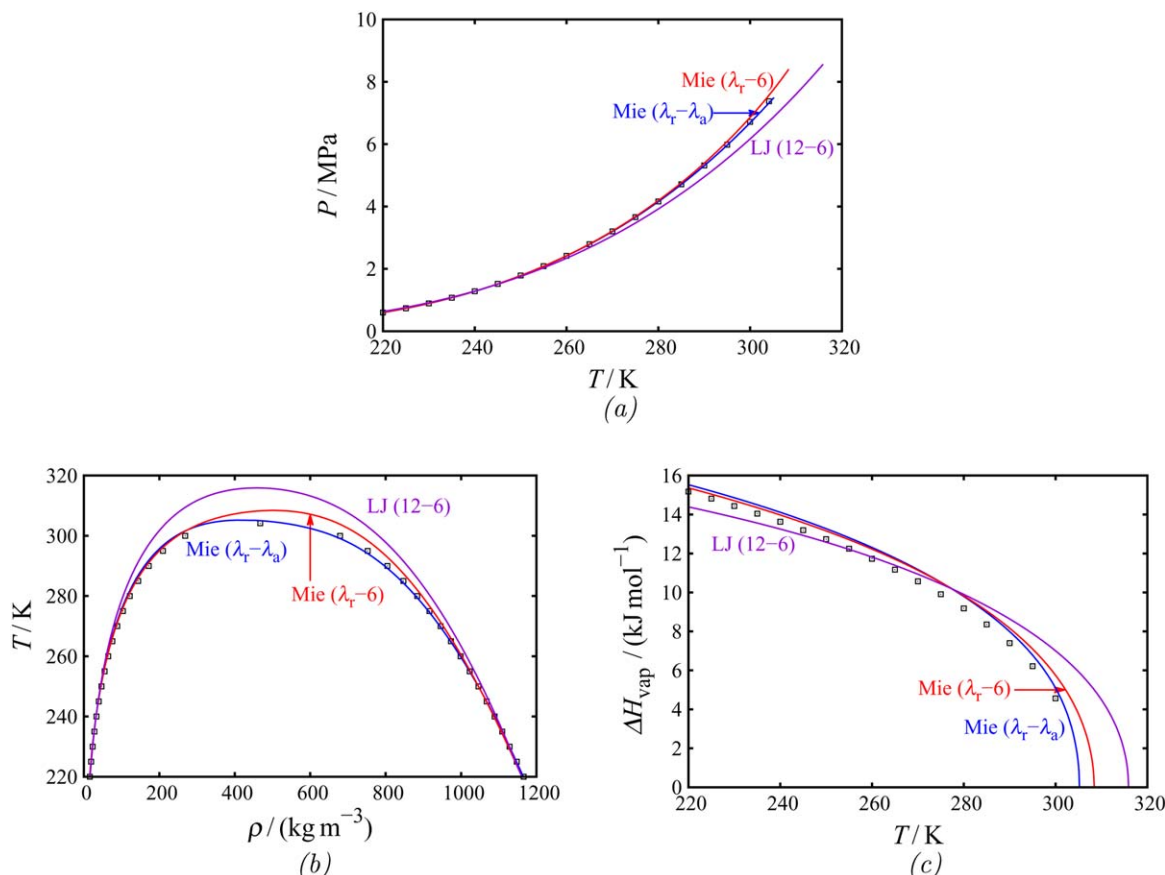
Figure 5. Performance of the different SAFT-VR Mie models based on the Lennard–Jones (12-6), Mie (λ_r-6), and generic Mie (λ_r-λ_a) potentials in relation to saturation properties of carbon dioxide: (a) vapor pressure; (b) saturated vapor and liquid densities; and (c) enthalpy of vaporization.

The symbols represent the correlated experimental data from NIST,[60] and the curves represent the description with the SAFT-VR Mie EOS[46]. [Color figure can be viewed in the online issue, which is available at wileyonlinelibrary.com.]

can be very simple with a single minimum or very complex with multiple local minima.

- Each plane in the multidimensional parameter space yields essentially equivalent results; consequently, one need investigate only a single plane for a pair of parameters in selecting an intermolecular-potential model.
- Different intermolecular-potential models are required to provide the very best descriptions of different properties, although parameter sets obtained by targeting a particular property may nevertheless perform well in respect of other properties.

In the remainder of the discussion, we will focus on obtaining models that are able to provide for a good description of VLE properties, that is, the models are selected based on their ability to represent the vapor pressure and saturated-liquid density of the pure components. A good description of the vapor pressure is an extremely important precursor to modelling multicomponent mixture fluid-phase behavior since the phase envelope of the mixture tends toward the vapor-pressure curve in the pure-component limit; any inaccuracy in the vapor pressure will result either in a poor description of the mixture or lead to unrealistic mixture parameters to compensate for bad pure-component models.

Developing SAFT-VR Mie models for other fluids

Models Based on LJ (12-6), Mie (λ_r-6), and Generic Mie (λ_r-λ_a) Potentials. To assess the overall performance of the SAFT-VR Mie EOS, we now develop intermolecular-

potential models for a wide range of compounds. The experimental data used in the parameter estimation are taken from the NIST[60] correlations in most cases except for the alkyl benzenes where the data are taken from Refs. 62–66. The conformal behavior of single-segment Mie fluids with the same value of α presented in Ref. 61 is again confirmed in Figure 4, for methane; this suggests that one can reproduce the behavior of the generic Mie (λ_r-λ_a) fluid using a Mie fluid of the same α with one of the exponents fixed to any value. In addition to our investigations in which both exponents are left free, we choose also to focus on the Mie (λ_r-6) family of fluids, characterized by a fixed value of the attractive exponent $\lambda_a = 6$. The value is chosen to match the exponent of the London dispersion interaction,[67] and can be reasonably taken as physically relevant for many fluids. To provide a reference for comparison, we consider also the more-familiar LJ (12-6) form of the Mie potential. We select the (λ_a, λ_r) plane as that on which to base our search for models. This choice enables us to highlight the advantages of the generic Mie potential over the more-widely used LJ (12-6) potential.

We focus first on carbon dioxide. The three models of carbon dioxide developed are based on a LJ (12-6), a Mie (λ_r-6), and a generic Mie (λ_r-λ_a) potential form. The parameters for each model are estimated using the same objective function (comprising the vapor pressure and saturated-liquid density of carbon dioxide, with equal weights, $\omega = 1$); in each

Table 1. Intermolecular Potential Models Developed for the *n*-Alkanes Using Mie (λ_r-6) Potentials; * Denotes That the Highlighted Parameter is Fixed at the Indicated Value During the Parameter Estimation

Substance	Molecular Parameters					%AAD						
	m	σ / Å	λ_r	λ_a	(ε/k_B) / K	d_{liq}	u	d_{sat}	p_{sat}	c_p	T_c	ΔH_{vap}
Methane	1.0000*	3.7366	12.319	6.0*	151.45	0.54	1.81	0.75	0.40	1.23	2.69	2.69
Methane[a]	1.0000*	3.7412	12.650	6.0*	153.36	0.74	1.97	0.75	0.63	2.03	2.41	2.87
Ethane	1.7230	3.4763	10.121	6.0*	164.27	0.53	5.75	0.40	0.44	2.59	2.27	1.49
Ethane[a]	1.4373	3.7257	12.400	6.0*	206.12	0.37	3.87	0.55	0.53	1.69	0.49	1.73
Propane	1.8068	3.7943	12.106	6.0*	221.96	0.59	9.39	0.67	0.77	2.24	1.68	1.44
Propane[a]	1.6845	3.9056	13.006	6.0*	239.89	0.51	4.76	0.93	0.44	2.40	1.44	1.41
Butane	1.6791	4.2476	15.453	6.0*	306.52	0.34	2.45	0.58	0.09	0.93	1.82	1.46
Butane[a]	1.8514	4.0887	13.650	6.0*	273.64	0.31	1.35	0.54	0.39	1.56	1.80	1.55
Pentane	1.8594	4.3759	16.438	6.0*	336.74	0.19	2.05	0.34	0.16	0.90	2.36	1.39
Pentane[a]	1.9606	4.2928	15.847	6.0*	321.94	0.32	1.65	0.52	0.60	0.68	2.85	1.67
Hexane	2.2549	4.2968	15.069	6.0*	321.81	0.29	1.83	0.29	0.16	0.87	2.47	1.68
Hexane[a]	2.1097	4.4230	17.203	6.0*	354.38	0.46	1.43	0.25	1.19	0.32	3.26	2.23
Heptane	2.2413	4.5427	18.252	6.0*	381.42	0.37	0.92	0.19	0.27	0.78	3.26	1.65
Heptane[a]	2.3949	4.4282	17.092	6.0*	358.51	0.39	0.67	0.45	0.91	0.91	3.52	1.79
Octane	2.4777	4.5708	18.654	6.0*	391.87	0.61	1.79	0.36	0.29	0.86	3.62	1.59
Octane[a]	2.6253	4.4696	17.378	6.0*	369.18	0.54	0.75	0.52	0.96	1.04	3.60	1.58
Nonane	2.6665	4.6236	19.116	6.0*	404.83	0.47	0.60	0.41	0.34	0.72	3.53	1.48
Nonane[a]	2.8099	4.5334	18.324	6.0*	387.55	0.43	0.45	0.60	0.82	0.63	3.77	1.60
Decane	3.0058	4.5727	18.403	6.0*	396.17	0.65	1.55	0.46	0.41	0.70	3.29	1.74
Decane[a]	2.9976	4.5890	18.885	6.0*	400.79	0.79	1.14	0.59	0.96	0.46	3.67	1.86
Dodecane	3.2483	4.7430	20.872	6.0*	438.20	0.68	1.22	0.43	0.56	0.95	3.52	1.78
Dodecane[a]	3.2519	4.7484	20.862	6.0*	437.72	0.64	0.92	0.52	0.59	0.95	3.56	1.73

The percentage absolute average deviation (%AAD) of the various properties calculated with the SAFT-VR Mie EOS[46] from the correlated experimental data of NIST[60] are indicated: single-phase liquid density d_{liq}; single-phase liquid speed of sound u; saturated-liquid density d_{sat}; vapor pressure p_{sat}; single-phase liquid isobaric heat capacity c_p; critical temperature T_c; enthalpy of vaporization ΔH_{vap}. Also included for comparison are models developed in Ref.46; these models were developed using p_{sat}, d_{sat}, T_c, ΔH_{vap}, d_{liq}, and u in the parameter estimation.
[a]Denotes models taken from Ref. 46.

case, the number of segments, m, is excluded from the parameter estimation and is assigned the fixed value $m = 1.6936$, which is estimated from quantum mechanical calculations for the size and nonsphericity parameters.[59]

The performance of the different models used to represent carbon dioxide in relation to saturation properties is illustrated in Figure 5. The model featuring a LJ (12-6) potential does not perform as well as the Mie (λ_r-6) model with a fixed attractive exponent of six, which itself performs less well than the Mie (λ_r-λ_a) model for which both exponents are estimated. One would, of course, expect such a result simply on the basis of the number of parameters: the model with the most adjustable parameters performs best. Accordingly, it is important to consider the respective adequacies of the models to assess whether the improvement in performance is due solely to the use of extra adjustable parameters.

The Mie (λ_r-λ_a) model obtained with variable repulsive λ_r and attractive λ_a exponents provides an excellent description of the VLE of carbon dioxide, but the physical significance of the exponents is not clear. This model is characterized by a value of $\lambda_a = 5.055$; the two leading contributions to the attractive intermolecular interactions of carbon dioxide are the London dispersion (which scales as $1/r^6$) and the quadrupole–quadrupole interaction (which scales as $1/r^8$), hence, it is difficult to account for an attractive exponent lower than six. A simple analysis of this type is however complicated by the fact that carbon dioxide is not spherical and possesses three atomic centers. Overall the Mie (λ_r-6) model offers a good compromise between the quality of the representation of the thermodynamic properties, the number of adjustable parameters, and the physical significance of these parameters.

In relation to the comparison between the different underlying potentials, similar results to those seen for carbon diox-

ide are obtained for other fluids. Accordingly, we favor in general those based on the Mie (λ_r-6) potential, which carry the London-dispersion attractive exponent. The SAFT-VR Mie parameters for the models obtained for the different fluids examined are presented in Tables 1–3, along with the %AAD values for different properties. Details relating to the experimental data used in the estimations, and the ranges of temperature and pressure considered, are given in Table 4. The models relating to the LJ (12-6) and generic Mie (λ_r-λ_a) potentials are presented in an Appendix (Tables A1–A2).

Fluid Models Based on Mie (λ_r-6) Potentials. The representation of the experimental data obtained using the SAFT-VR Mie EOS is found to be very good. This is illustrated for the case of Mie (λ_r-6) models for the VLE (saturated vapor and liquid densities, vapor pressure, and enthalpy of vaporization) of *n*-alkanes from methane to *n*-decane and *n*-dodecane in Figure 6, and for other common fluids in Figure 7 (the model parameters can be found in Tables 1–3). The quality of the description of the enthalpy of vaporization (Figures 6c and 7c) is particularly gratifying. We note also that the versatility of the models and theory is evident from the diversity of molecules that are very well described.

A noteworthy feature common to all the models is a relatively small overestimate of the critical point, compared to that obtained with the previous formulations of SAFT-VR and with other SAFT EOS; this improved performance in the near-critical region enables a much better description of the saturation densities. This feature will simplify the modelling of mixtures where one or more components is just supercritical. Conditions at which the real fluid is supercritical but at which the model fluid is subcritical necessarily create difficulties in the description of mixtures; for example, phase diagrams in composition space have a fundamentally

Table 2. Intermolecular Potential Models Developed for Various Hydrocarbons Using Mie (λ_r-6) Potentials; * Denotes That the Highlighted Parameter is Fixed at the Indicated Value During the Parameter Estimation

Substance	Molecular Parameters					%AAD						
	m	σ / Å	λ_r	λ_a	(ε/k_B) / K	d_{liq}	u	d_{sat}	p_{sat}	c_p	T_c	ΔH_{vap}
Benzene	2.2785	3.7806	11.594	6.0*	297.53	0.52	3.47	0.22	0.35	2.32	1.97	2.30
Benzene[a]	1.9163	4.0549	14.798	6.0*	372.59	0.44	2.33	0.34	0.89	1.95	2.80	2.46
Cyclohexane	2.1641	4.1071	12.412	6.0*	313.04	0.56	4.79	0.17	0.30	2.31	1.53	3.28
Cyclopropane	1.8769	3.4830	10.507	6.0*	213.11	0.63	4.97	0.02	0.07	2.38	2.56	4.54
Dimethylpropane	1.0000*	5.6491	31.792	6.0*	504.25	0.93	5.81	0.14	0.65	2.56	2.97	3.27
Ethylene	1.7972	3.2991	9.6463	6.0*	142.64	0.54	3.56	0.37	0.52	4.18	2.07	1.66
Isobutane	1.7186	4.2177	14.612	6.0*	281.12	0.43	8.43	0.62	0.36	1.70	2.11	1.48
Isohexane	2.2759	4.2839	14.756	6.0*	307.74	0.53	4.80	0.40	1.48	4.74	3.18	1.53
Isopentane	1.7464	4.4714	16.688	6.0*	339.95	0.28	2.27	0.37	0.27	0.85	2.40	1.17
Propylene	2.0060	3.5392	10.643	6.0*	190.13	0.62	5.01	0.55	0.78	2.57	1.57	1.50
Propyne	2.3038	3.2076	10.667	6.0*	200.11	0.31	6.45	0.16	0.53	7.00	2.89	4.54
Toluene	1.7112	4.5487	19.125	6.0*	474.13	0.35	3.44	0.46	0.20	1.15	1.74	1.82
Toluene[a]	1.9977	4.2777	16.334	6.0*	409.73	0.28	2.25	0.46	1.46	1.91	2.96	2.15
Ethyl-benzene	2.3501	4.2436	15.241	6.0*	386.09	–	–	2.85	0.60	–	–	–
Propyl-benzene	2.7357	4.1999	12.853	6.0*	342.41	–	–	2.66	0.17	–	–	–
Butyl-benzene	2.9762	4.2522	13.237	6.0*	350.48	–	–	3.50	0.19	–	–	–
Pentyl-benzene	3.0488	4.3881	15.594	6.0*	394.46	–	–	1.47	0.50	–	–	–
Decyl-benzene	4.0808	4.5745	17.746	6.0*	431.37	–	–	3.29	0.42	–	–	–

The %AAD of the various properties calculated with the SAFT-VR Mie EOS[46] from the correlated experimental data of NIST[60] are indicated: single-phase liquid density d_{liq}; single-phase liquid speed of sound u; saturated-liquid density d_{sat}; vapor pressure p_{sat}; single-phase liquid heat capacity c_p; critical temperature T_c; enthalpy of vaporization ΔH_{vap}. Also included for comparison are models developed in Ref. 46; these models were developed using p_{sat}, d_{sat}, T_c, and u in the parameter estimation.
[a]Denotes models taken from Ref. 46.

different shape when one or more component becomes supercritical.

It is interesting to examine the variation in the repulsive exponent, λ_r, obtained for the different fluids; the exponent takes values ranging from less than 9 for O_2 to $\sim$37 for SF_6. The very hard repulsive nature of the potential obtained for SF_6 is rationalized by considering the highly electronegative nature of fluorine, whereby one expects very strong repulsions between fluoride ligands on separate molecules; in similar fashion, a very steeply repulsive potential was required to obtain a good representation of CF_4.[46] The values of λ_r for the remaining molecules lie generally in the range $(9 \lesssim \lambda_r \lesssim 20)$. The exception is dimethyl propane, for which $\lambda_r \sim 32$ is obtained; here the hardness of the potential

may reflect the steric hindrance to molecular deformation of the closely positioned methyl groups on the molecule, although we note that the shape parameter was constrained to a value $m = 1.0$ during the parameter estimation, so the anomalously high value of λ_r could also indicate that this restriction is too severe.

For many years, it has been common practice to use the standard LJ (12-6) potential, almost by default. With this in mind, if one compares the models presented in Tables 1–3 with those in Tables A1–A3 (in the Appendix), for which the LJ (12-6) form is enforced, some of the Mie (λ_r-6) models perhaps appear surprising in terms of the magnitudes of λ_r and ε that one encounters. However, this does not mean that our featured Mie models are nonphysical. On the

Table 3. Intermolecular Potential Models Developed for Various Compounds Using Mie (λ_r-6) Potentials; * Denotes That the Highlighted Parameter is Fixed at the Indicated Value During the Parameter Estimation

Substance	Molecular Parameters					%AAD						
	m	σ / Å	λ_r	λ_a	(ε/k_B) / K	d_{liq}	u	d_{sat}	p_{sat}	c_p	T_c	ΔH_{vap}
Ar	1.0000*	3.4038	12.085	6.0*	117.84	0.49	2.13	0.66	0.21	1.77	2.19	3.09
CO	1.5556	3.0928	9.7420	6.0*	72.110	0.32	2.39	0.15	0.08	2.64	1.54	1.27
CO_2	1.6936	3.0465	18.067	6.0*	235.73	0.85	16.86	0.3	0.12	3.45	2.69	3.08
COS	1.8746	3.2978	9.5435	6.0*	186.38	0.59	3.96	0.38	0.74	3.46	2.30	1.84
F_2	1.5094	2.8118	9.9255	6.0*	80.803	0.36	5.73	0.25	0.02	2.04	1.58	1.25
F_2[a]	1.3211	2.9554	11.606	6.0*	96.268	0.31	4.52	0.50	0.44	1.47	0.61	1.51
Kr	1.0000*	3.6359	11.985	6.0*	163.27	0.57	2.33	0.69	0.19	0.89	2.35	3.32
N_2	1.4214	3.1760	9.8749	6.0*	72.438	0.46	2.71	0.15	0.07	2.31	0.06	1.43
N_2O	2.0526	2.8440	10.930	6.0*	163.69	0.51	7.20	0.09	0.04	2.03	2.13	2.99
Ne	1.0000*	2.8019	9.6977	6.0*	29.875	0.45	6.57	0.06	0.43	4.56	1.69	2.02
NF_3	1.8196	3.2069	10.764	6.0*	128.73	0.48	7.20	0.31	0.34	2.81	1.67	1.81
O_2	1.4283	2.9671	8.9218	6.0*	81.476	0.55	5.08	0.39	0.24	2.76	1.89	1.04
SF_6	1.0000*	4.8768	36.696	6.0*	381.99	0.96	5.78	0.07	0.41	6.25	2.29	4.29
SO_2	2.4599	2.8511	11.865	6.0*	225.73	0.69	15.17	0.11	0.16	3.10	1.96	2.88
Xe	1.0000*	3.9612	12.275	6.0*	229.47	0.63	2.86	0.74	0.19	1.16	2.55	3.63

The %AAD of the various properties calculated with the SAFT-VR Mie EOS[46] from the correlated experimental data of NIST[60] are indicated: single-phase liquid density d_{liq}; single-phase liquid speed of sound u; saturated-liquid density d_{sat}; vapor pressure p_{sat}; single-phase liquid heat capacity c_p; critical temperature T_c; enthalpy of vaporization ΔH_{vap}. Also included for comparison are models developed in Ref. 46; these models were developed using p_{sat}, d_{sat}, T_c, ΔH_{vap}, d_{liq}, and u in the parameter estimation.
[a]Denotes models taken from Ref. 46.

Table 4. Ranges of Temperature T and Pressure p of the Experimental Data Incorporated in the Parameter Estimations During the Development of Models, and for the Determination of the %AAD of the Various Properties Calculated with the SAFT-VR Mie EOS[46] from the Correlated Experimental Data for Each Fluid

Substance	Vapor-liquid equilibrium		Compressed-liquid phase		
	T range (K)	♯(Data points)	T range (K)	p range (MPa)	♯(Data points)
Methane	95–185	21	100–190	10–50	30
Ethane	95–275	37	100–300	10–50	33
Propane	90–330	49	100–360	10–50	42
Butane	135–380	50	140–420	10–50	44
Pentane	145–420	56	150–450	10–50	31
Hexane	180–455	56	200–500	10–50	32
Heptane	185–485	61	200–530	10–50	35
Octane	220–510	59	230–560	10–50	35
Nonane	220–535	64	230–560	10–50	34
Decane	245–555	63	300–600	10–50	33
Dodecane	265–590	66	290–650	10–50	38
Cyclohexane	280–495	44	300–560	10–50	38
Cyclopropane	275–355	17	290–390	10–28	30
Dimethylpropane	260–390	27	270–430	10–50	44
Ethylene	105–250	30	110–280	10–50	53
Isobutane	115–365	51	125–405	10–35	45
Isohexane	125–445	65	130–490	10–50	38
Isopentane	115–410	60	120–460	10–50	53
Propylene	100–325	46	120–360	10–50	39
Propyne	275–360	18	280–400	10–30	36
Benzene	280–505	46	300–560	10–50	41
Toluene	180–530	71	190–590	10–50	62
Ethyl-benzene[64,65]	183–518	24	–	–	–
Propyl-benzene[64,65]	223–543	15	–	–	–
Butyl-benzene[64,65]	223–583	13	–	–	–
Pentyl-benzene[64,65]	223–593	10	–	–	–
Decyl-benzene[62,63,65,66]	318–633	12	–	–	–
Ar	85–135	11	90–150	10–50	20
CO	70–115	10	75–130	10–50	35
CO_2	220–270	22	220–300	10–50	50
COS	135–340	42	155–375	10–50	36
F_2	55–125	15	60–140	10–20	27
Kr	120–185	14	120–200	10–50	24
N_2	65–110	10	75–125	10–100	23
N_2O	185–275	19	195–305	10–50	34
Ne	24–40	16	29–45	10–50	20
NF_3	85–210	26	95–225	10–50	41
O_2	55–135	17	60–150	10–50	30
SF_6	225–285	13	235–315	10–55	22
SO_2	200–385	38	220–420	10–35	33
Xe	165–260	20	175–285	10–50	35

Also provided are the numbers of data points used. The correlated experimental data are taken from the NIST database,[60] except for the alkyl benzenes, for which the sources of data are indicated by the cited references.

contrary; the improved predictive power of the models evidenced by the reduction in %AAD from experimental data for second-derivative properties (in particular, for speeds of sound) suggests that the models have a firmer physical foundation. As a final comment on the values obtained for λ_r, it is interesting to find that, with the exception of neon (which is influenced by quantum effects and imperfectly described using the LJ (12-6) form without quantum correction[68–70]) the noble gases are generally well described using a potential that is essentially of the LJ (12-6) form.

Versatility of models obtained using vapor-liquid saturation properties

As illustrated in previous work,[46,48,49,71] the SAFT-VR Mie EOS offers the simultaneous capability of an accurate description of the VLE and second-derivative properties (such as speed of sound or heat capacity) of fluids. This feature is very useful as it widens the applicability of the EOS, as well as providing confidence that the theory and the

resulting models are physically sound. Although the $(\lambda_r\text{-}6)$ Mie models we obtain are based on an objective function comprising the vapor pressures and saturated-liquid densities (with equal weight), a good overall description of the single-phase densities and second-derivative properties of many different fluids is provided, as can be seen from the %AAD from the experimental data[60] given in Tables 1–3 (analogous tables relating to the LJ (12-6) and generic Mie $(\lambda_r\text{-}\lambda_a)$ models are given in the Appendix).

Further demonstration is provided graphically in Figures 8–10, in which descriptions of single-phase isobaric properties of carbon dioxide, xenon, and isopentane (respectively) are provided for illustration; the properties examined include the single-phase density, the Joule–Thomson coefficient, the isobaric heat capacity, and the speed of sound. (Essentially equivalent performance is found using the models obtained for the other fluids.) As can be seen from these figures, the descriptions of the various properties provided by these models are excellent throughout, notwithstanding that none of these properties were included in the objective functions
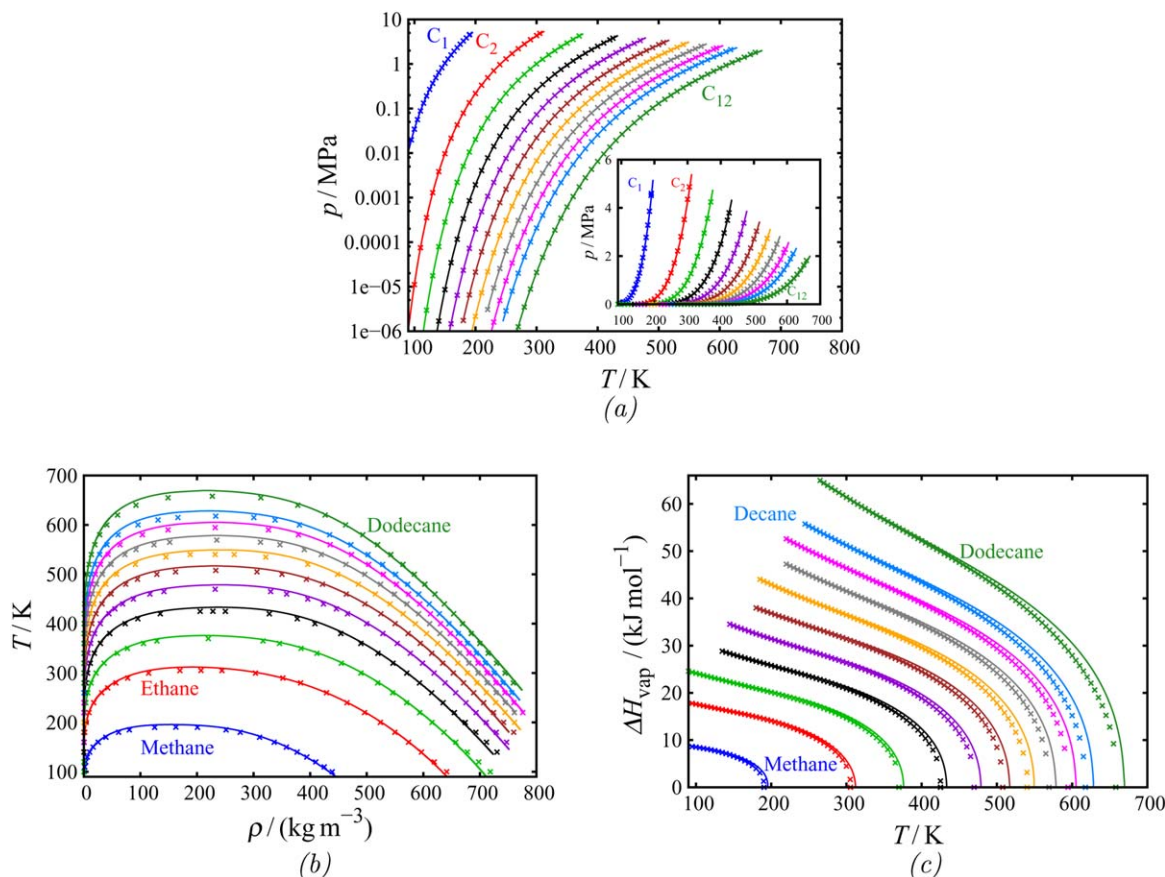
Figure 6. Performance of the SAFT-VR Mie EOS[46] in relation to saturation properties of the _n_-alkanes: (a) vapor pressure; (b) saturated vapor and liquid densities; and (c) enthalpy of vaporization.

The symbols represent correlated experimental data from NIST,[60] and the curves represent the description with the Mie (λ_r-6) models presented in Table 3. [Color figure can be viewed in the online issue, which is available at wileyonlinelibrary.com.]

used in parameter estimation; as discussed earlier for methane, an enhanced description may be obtained if the properties are targeted in the parameter estimation (though probably at the expense of a slightly poorer description of the VLE). It is also interesting to note that, in separate work[72] using models for _n_-butane and _n_-decane developed previously in Ref. 46 (also provided in Table 1 for completeness), excellent predictions were obtained for the fluid-phase equilibria of these two compounds in both the temperature–entropy (T, S) and pressure–enthalpy (p, H) projections.

Homologous series: Trends in the characteristic parameters of the models

When appropriately combined, the parameters used in SAFT-VR Mie for molecules in homologous series exhibit clear physical trends, reflecting the molecular basis of the theory. This was first explored within the context of SAFT by Huang and Radosz,[16] who examined the molecular weight (MW) dependence of the molecular length m, segment volume, and segment energies for alkanes and polynuclear aromatics. The idea was exploited to obtain parameters for polyethylene by correlating the trends observed for low-MW alkanes and extrapolating to high MW. Similar procedures have been adopted to procure model parameters for polymers within other SAFT frameworks, for example, in Refs. 73 and 74 (for SAFT-VR),[22] Ref. 75 (for PC-SAFT),[26] and Ref. 76

(for soft-SAFT).[24] The numerous successful studies of thermodynamic properties of polymers in which such models have been used collectively demonstrate the reliability of the concept; these include, for example, the studies presented in Refs. 26,73–88.

In our case, we focus on the _n_-alkanes using the Mie (λ_r-6), LJ (12-6), and generic Mie (λ_r-λ_a) models presented in Tables 1, A1, and A4, respectively, and the _n_-alkyl benzenes using the Mie (λ_r-6) models given in Table 2 (note that we have not developed LJ or generic Mie models for the alkyl benzenes). The individual parameters themselves do not necessarily follow clear relationships, although there is an increasing trend in the values of λ_r as evidenced in Table 1 for the _n_-alkanes, excluding methane. The fundamental physics that allows these models to perform so well reappears when considering appropriate combinations of parameters. A useful combination of parameters is the molecular volume, characterized by $\mathcal{V}=m\sigma^3$, which is found to be linear with the number of carbon atoms for the three families of models for the _n_-alkanes and also for the Mie (λ_r-6) models of the _n_-alkyl-benzenes, as seen in Figure 11a. This volumetric parameter takes into account the very strong coupling between the chain length m and the segment diameter σ, and is found to be quite constant for a given component, as seen previously in Figure 3. The other physically meaningful parameter combination of
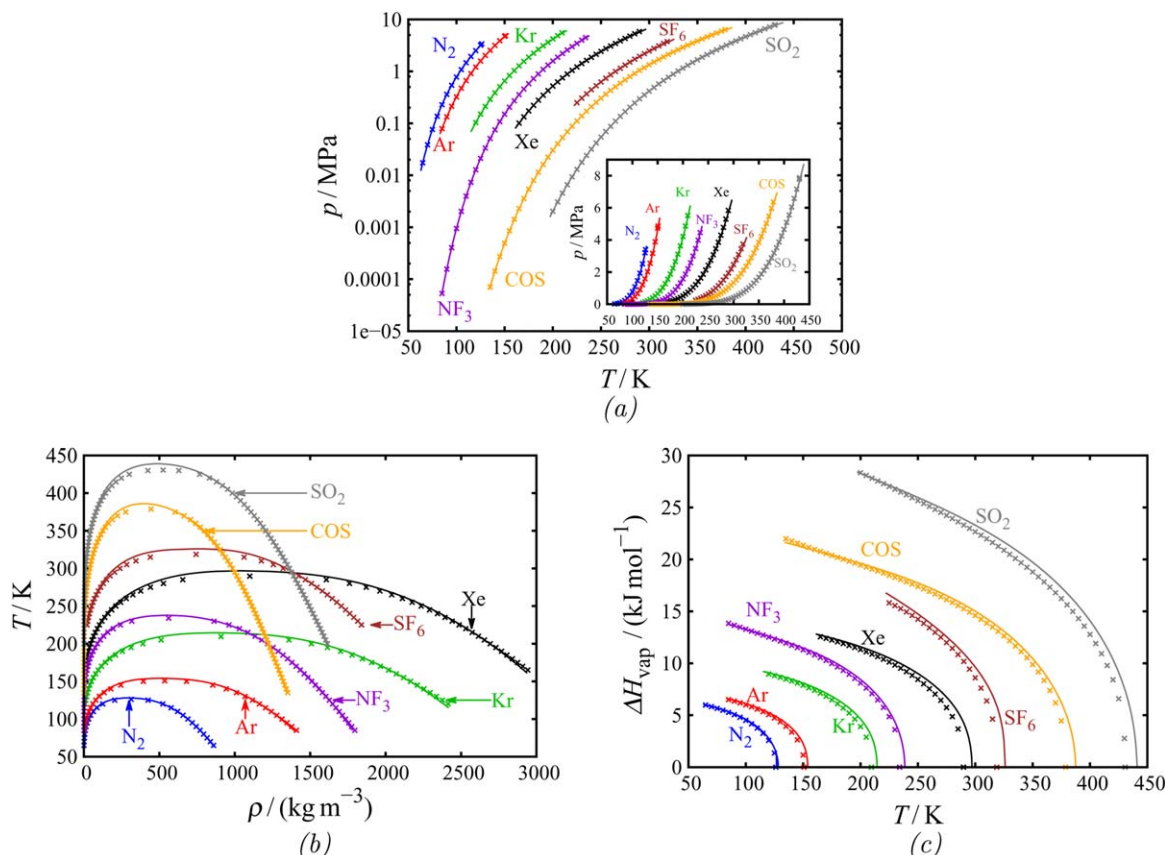
Figure 7. Performance of the SAFT-VR Mie EOS[46] in relation to saturation properties of various compounds: (a) vapor pressure, (b) saturated vapor and liquid densities, and (c) enthalpy of vaporization.

The symbols represent correlated experimental data from NIST,[60] and the curves represent the description with the Mie (λ_r-6) models presented in Table 3. [Color figure can be viewed in the online issue, which is available at wileyonlinelibrary.com.]

interest is the integrated van der Waals-like attractive energy E_{int} of the molecule, defined in Eq. 31. This energetic parameter is found to vary as a second-degree polynomial of the number of carbons, as can be seen in Figure 11b: such a quadratic dependence is expected from the dependence of E_{int} on the square of the molecular length, m^2. Although one cannot directly determine a model using these relationships as there are more parameters than equations, they can be used to determine a good starting guess for the estimation. More importantly, the existence of the trends is a further testament to the manner in which theory and models capture the physical characteristics of the molecules.

Discussion and Conclusions

It was demonstrated in Ref. 46, using detailed comparisons with molecular simulation, that the new formulation of SAFT-VR Mie performs extremely well in describing the physics of Mie (generalized LJ) fluids; the close agreement between thermodynamic properties calculated with the theory and those obtained in simulations is remarkable. However, although excellent models for real fluids were developed, a detailed examination of the model parameter space was not conducted and, accordingly, it remained to gain the insight necessary to be able to best exploit the enhanced capability of the new theory in terms of developing models to represent real fluids. In this work, this has

been addressed in relation to nonassociating fluids; our extension of this investigation to associating fluids is presented in a separate publication.[51]

To identify the most-appropriate models for real fluids one requires an appreciation of the sensitivity of calculated properties to changes in the values of the intermolecular potential model parameters; in related fashion, one needs also to understand and be able to resolve any issues associated with model degeneracy, whereby different models provide apparently equivalent performance. Degeneracy has been reported previously with respect to models based on the SW potential (with three adjustable parameters),[52,53] and is, therefore, expected when using models based on the Mie potential, which is characterized by four parameters. Here, we have carried out a detailed examination of the parameter space for models of nonassociating molecules, as exemplified in contour plots of the landscapes of objective functions (based on the square residual differences between experimental and calculated properties) projected onto different planes of parameter space. Even for an apparently simple molecule such as methane, the parameter space is seen to be quite complex, and therefore, identifying "the best" model for a compound is not straightforward. Model degeneracy is indeed encountered; the objective-function landscape features valleys within which many high-fidelity models may be located. The number of these valleys, and their location, depends on the properties included in the objective function; consequently, even though performance is generally good
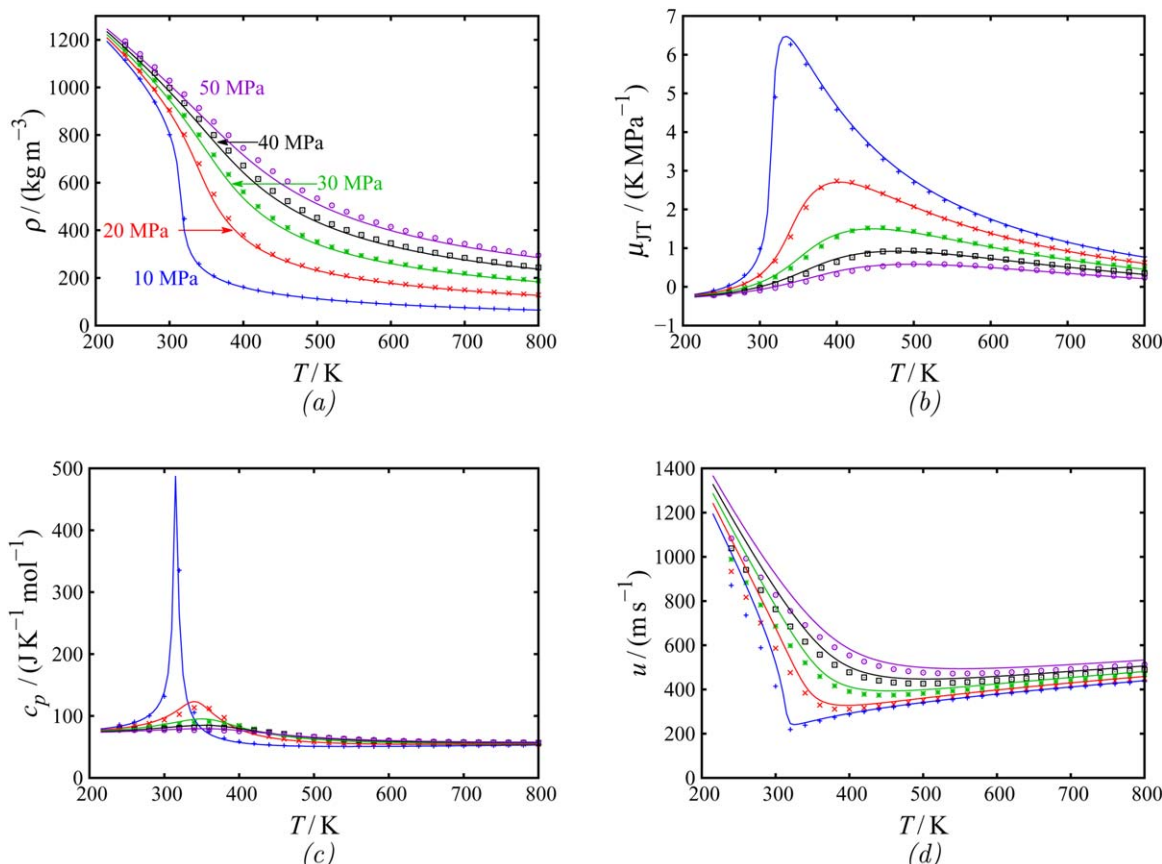
Figure 8. Prediction of single-phase isobaric properties of carbon dioxide with the SAFT-VR Mie EOS[46]: (a) compressed-liquid density, (b) Joule–Thomson coefficient, (c) isobaric heat capacity, and (d) speed of sound, at p = 10, 20, 30, 40, and 50 MPa.

The symbols represent correlated experimental data from NIST,[60] and the curves represent the description with the Mie (λ_r-6) model of carbon dioxide presented in Table 3. [Color figure can be viewed in the online issue, which is available at wileyonlinelibrary.com.]

over a wide range of properties, the optimal descriptions of particular properties are obtained using property-specific models. Additionally, these valleys may extend over large regions of the landscape and although a mathematically optimal parameter set may be found (as judged by the value of the objective function), this model may be characterized by physically unreasonable values of molecular parameters, whereas the valleys may contain other only marginally poorer models characterized by physically sensible parameter values—models that may themselves have been "optimal" given a slightly different choice of the form of the objective function. Thus it is important not to rely blindly on a simple optimization to estimate parameters for an intermolecular potential model of a fluid. Rather, one should use knowledge of the physical nature of the molecule to inform the estimation procedure; for example, in the case of a simple molecule such as methane, a physically reasonable model is expected to be characterized by an attractive exponent of λ_a = 6, following London dispersion, and m = 1, that is, a single spherical core—and we have seen that assigning these values does indeed assist in discriminating between the many good models of methane. From a different perspective, this means that one can assign parameters based on physical considerations and still obtain excellent models.

To examine the objective-function landscape in every possible plane of the parameter space is a labor-intensive and time-consuming task. From our examination of the parameter space of models of methane, we find that it is sufficient to consider only a single plane; this conclusion is born out in subsequent studies of other fluids. We favor the (λ_a, λ_r) plane defining the attractive and repulsive exponents of the Mie potential form, which facilitates simpler comparisons with models based on the more-familiar LJ (12-6) potential. It has been shown in Ref. 61 that two spherical Mie fluids of the same α (see Eq. 16) have the same free energy, and hence, the same thermodynamic properties; this was also demonstrated in our current work, in Figure 4. Accordingly a suitable procedure for developing models can be summarized as comprising a detailed examination of the parameter space in the (λ_a, λ_r) plane, using an objective function tailored to include properties that are of the greatest importance for the purpose at hand, while using knowledge of the physical nature of the molecule and the conformal behavior of Mie fluids of the same α to discriminate between near-degenerate models.

Using the strategy we have prescribed, models have been developed for a wide range of fluids, based not only on the generic Mie (λ_r-λ_a) potential (in which both exponents are free to vary), but also on the Mie (λ_r-6) form (for which the attractive exponent, λ_a, is constrained to the London-dispersion value of six), and the Mie (12-6) form, commonly known as the LJ potential; the experimental data used in the parameter-estimation procedure comprised saturation properties including the vapor-pressure and saturated-liquid density,
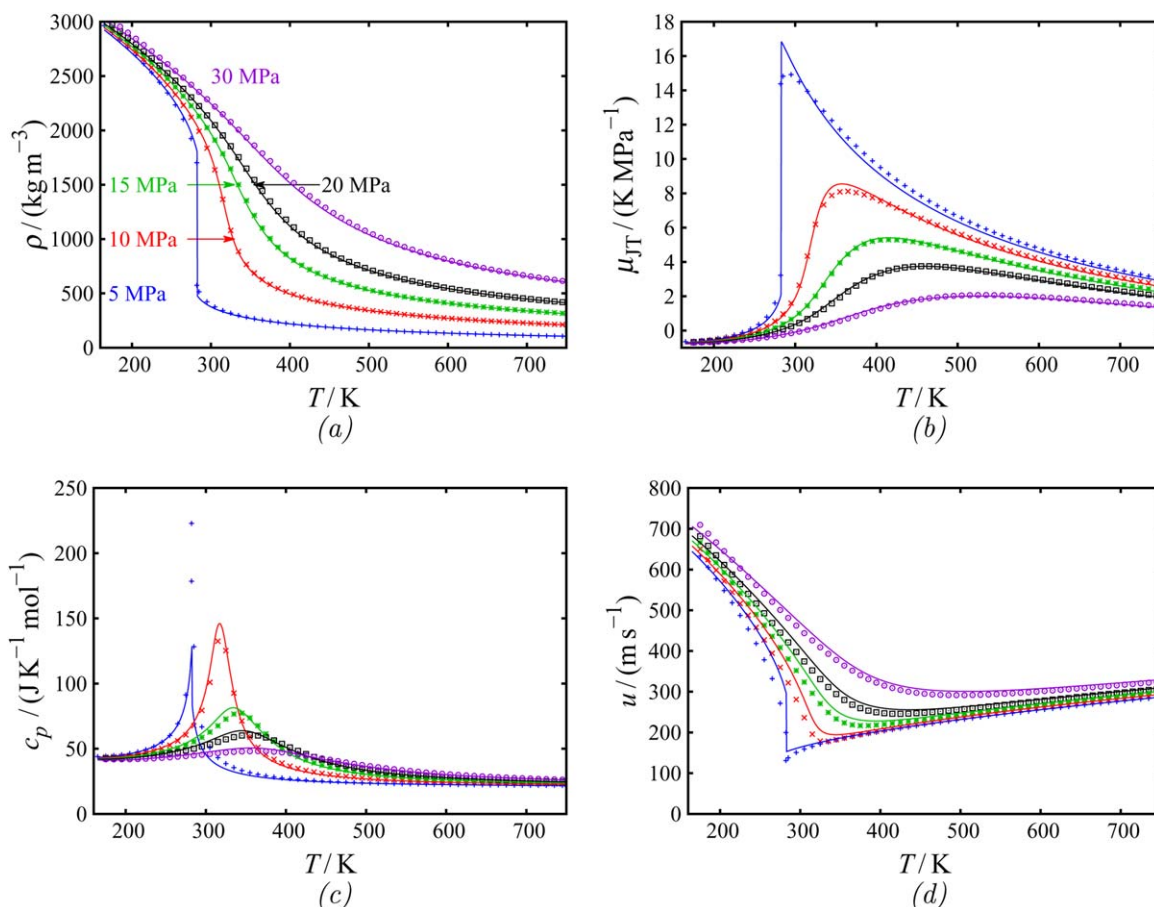
Figure 9. Prediction of single-phase isobaric properties of xenon with the SAFT-VR Mie EOS[46]: (a) compressed-liquid density, (b) Joule–Thomson coefficient, (c) isobaric heat capacity, and (d) speed of sound, at $p = 5$, 10, 15, 20, and 30 MPa. The symbols represent correlated experimental data from NIST,[60] and the curves represent the description with the Mie (λ_r-6) model of xenon presented in Table 3.

[Color figure can be viewed in the online issue, which is available at wileyonlinelibrary.com.]

chosen since in this work, the suitability of the models for use in studying mixture fluid-phase equilibria is of key importance. (For more-general work, one might prefer models in which some single-phase properties are targetted, such as the liquid density or heat capacity.) In conjunction with the SAFT-VR Mie EOS,[46] the resulting models provide an excellent description of a variety of thermophysical properties of the chosen fluids, including single-phase and second-derivative properties not included in the model development.

When comparing models based on the different potentials, generic Mie (λ_r-λ_a) models are seen to provide the best performance though the difference in quality between these and the Mie (λ_r-6) models is not very significant—which is consistent with our earlier observation of conformality of Mie fluids (which implies that one can always find a Mie (λ_r-6) model with the same integrated energy parameter α as the generic Mie form, that will provide similar performance). Of the three classes of model, those based on the LJ (12-6) potential performed least well on average. Some fluids, exemplified by the Mie models of SF_6 or dimethylpropane, are not well represented with LJ models; SF_6, in particular, requires a very repulsive potential. Conversely, in some particular cases, such as the noble gases argon, krypton, and xenon, the performance of the LJ models was just as good as that of the generic Mie potential. (Given the ubiquitous use of the LJ potential in both theory and simulation, it is

reassuring to see how well LJ models can work in comparison with the more-versatile Mie models but, at the same time, it is very useful to be able to assess when such a model may not be appropriate.) Based on these comparisons and the foregoing discussion, for nonassociating molecules of the type considered here we favor models based on the Mie (λ_r-6) form, since the potential offers an excellent compromise between the number of adjustable parameters, respect of the physical nature of the molecules, and overall performance of the model.

The adequacy of our models in accurately capturing the saturation properties is seen to be outstanding, in the context of modelling using a theoretically based EOS (as opposed to a detailed mathematical correlation, such as the Span and Wagner[89] EOS for carbon dioxide). There is discernibly a significant improvement compared with the performance available using the previous formulation of SAFT-VR[22] with available models. Especially noteworthy is the greatly reduced "overshoot" of the critical point; previously, such good performance simultaneously for both the subcritical and near-critical regions using an analytical EOS had been possible only with the incorporation of a cross-over treatment, such as those of Refs. 90–93.

For most problems of practical interest, one seeks to model not only pure-component fluids, but mixtures—often containing many components. The excellence of the description
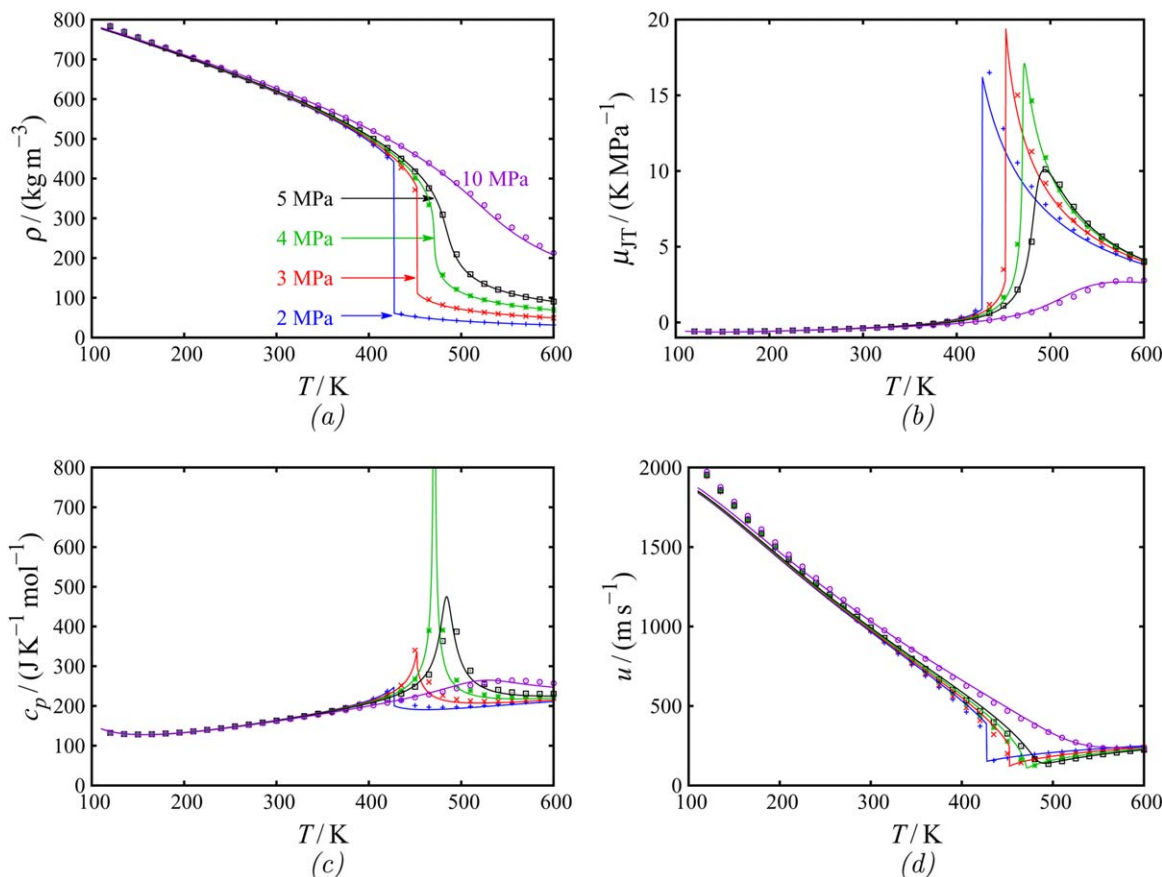
Figure 10. Prediction of single-phase isobaric properties of isopentane with the SAFT-VR Mie EOS[46]: (a) compressed-liquid density, (b) Joule–Thomson coefficient, (c) isobaric heat capacity, and (d) speed of sound, at $p = 2$, 3, 4, 5, and 10 MPa. The symbols represent correlated experimental data from NIST,[60] and the curves represent the description with the Mie (λ_r-6) model of isopentane presented in Table 3.

[Color figure can be viewed in the online issue, which is available at wileyonlinelibrary.com.]

of pure-component saturation properties provides confidence that the fluid-phase equilibria of mixtures, based on these pure-component models, will in turn be well described. For example, one cannot obtain a good representation of the isothermal pressure-composition or isobaric temperature-composition phase diagrams of binary mixtures if one cannot first describe well both pure-component limits, that is, the vapor-pressure curves. On this basis alone, one can anticipate that the modelling of the fluid-phase equilibria of mixtures with the SAFT-VR EOS will be of equivalent quality to that of the pure components. However, by setting out a clearly prescribed strategy for pure-component model development, such as that laid out here, one can ensure that all of the pure-component models from which mixture models may later be developed are themselves developed in a consistent manner, thereby providing extra confidence that one will obtain a coherent and high-quality description of the properties of the fluid mixture.

Although the models developed in our current work are homonuclear models based on molecular segments described with the Mie potential, it is important to note that they may be used seamlessly with the SAFT-γ Mie EOS,[37,38] in which generic heteronuclear molecular models formed from different types of fused Mie segments are considered. For example, the CO_2 model developed here can be used in a GC methodology in modelling mixtures with hydrocarbons. Moreover, the generality of our models extends beyond their use in EOS model-

ling. The faithful representation of the thermodynamic properties of Mie fluids with the SAFT-VR Mie[46] allows the same models to be used in coarse-grained molecular simulations; thereby interfacial and transport properties, or other properties that are not directly accessible using the EOS, may be determined. Successful examples of coarse-grained simulations based on SAFT-VR Mie and SAFT-γ Mie models are described in, for example, Refs. 71,94−100.

In the Introduction, we noted the trend in modern engineering practice toward a demand for EOSs that provide a simultaneous description of a wider variety of thermophysical properties, that is, an all-encompassing representation of the thermodynamics of a fluid, and we return to this point in closing. Although our models were developed using only saturation properties, their performance in respect of the description they allow for other thermodynamic properties is nevertheless excellent. This has been exemplified in this work for the single-phase compressed liquid density, enthalpy of vaporization, Joule–Thomson coefficient, speed of sound, and isobaric heat capacity, and, in a recent publication,[72] for a representation of the saturation properties in the (T, S) and (p, H) projections of the vapor-liquid equilibria. The capacity of the new SAFT-VR Mie EOS to simultaneously provide such high-quality descriptions of numerous thermodynamic properties in a simultaneous manner represents a tremendous advance in generalized EOS modelling of fluids.
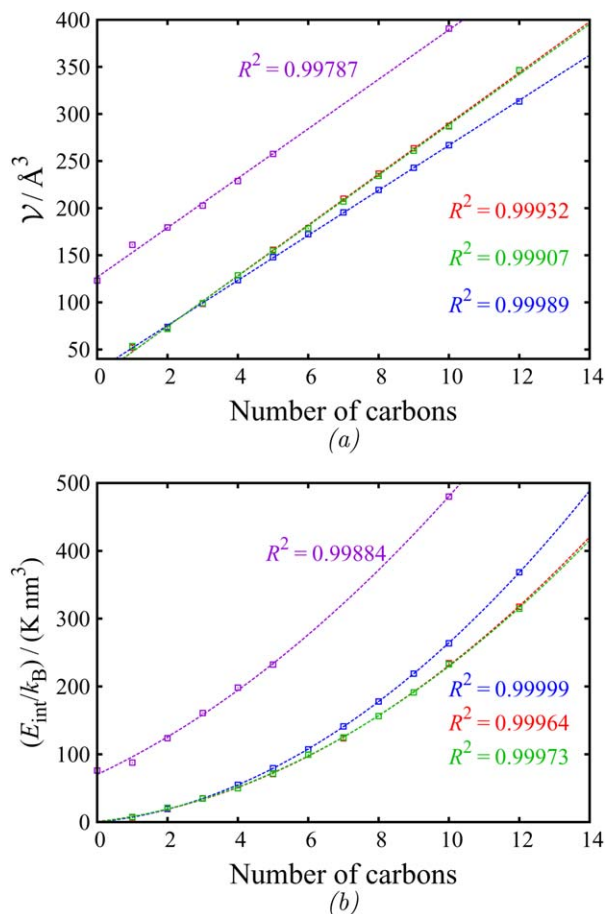
Figure 11. Trends in (a) the molecular volume $\mathcal{V}=m\sigma^3$, and (b) the integrated van der Waals-like attractive energy $E_{int}=m^2\sigma^3\epsilon\alpha$ for the models of the n-alkanes and n-alkyl benzenes; blue corresponds to Lennard–Jones (12-6) models, red to Mie (λ_r-6) models, and green to models based on the generic Mie (λ_r-λ_a) potential for the n-alkane family; purple corresponds to the Mie (λ_r-6) models for the n-alkyl benzene family. The values of R^2 represent the square of the Pearson product-moment correlation coefficient for the fits represented by the dashed curves (linear for the molecular volume, second degree polynomial for the integrated energy).

[Color figure can be viewed in the online issue, which is available at wileyonlinelibrary.com.]

Acknowledgments

Literature Cited

1. Prausnitz JM, Lichtenthaler RN, de Azevedo EG. *Molecular Thermodynamics of Fluid-Phase Equilibria*. Upper Saddle River, New Jersey, USA: Prentice Hall, 3rd ed. 1999.
2. Redlich O, Kwong JNS. On the thermodynamics of solutions. V An equation of state. Fugacities of gaseous solutions. *Chem Rev.* 1949; 44:233–244.
3. van der Waals JD. Over de Continuiteit van den Gas-en Vloeistof-toestand. Ph.D. thesis, *Leiden.* 1873.
4. van der Waals JD. *On the Continuity of the Gaseous and Liquid States.* Dover Pheonix edition. Dover Publications, Mineola, N. Y. 2004. English translation, Rowlinson JS; originally published as Volume XIV in series *Studies in statistical mechanics*, Amsterdam: North-Holland Physics Publishing, 1988.
5. Soave G. Equilibrium constants from a modified Redlich-Kwong equation of state. *Chem Eng Sci.* 1972;27:1197–1203.
6. Peng DY, Robinson DB. A new two-constant equation of state. *Ind Eng Chem Fundam.* 1976;15:59–64.
7. Kontogeorgis GM, Folas GK. *Thermodynamic Models for Industrial Applications.* UK: Wiley, 2010.
8. Chapman WG, Gubbins KE, Jackson G, Radosz M. SAFT: equation-of-state solution model for associating fluids. *Fluid Phase Equilib.* 1989;52:31–38.
9. Chapman WG, Gubbins KE, Jackson G, Radosz M. New reference equation of state for associating liquids. *Ind Eng Chem Res.* 1990; 29:1709–1721.
10. Wertheim MS. Fluids with highly directional attractive forces. I. Statistical thermodynamics. *J Stat Phys.* 1984;35:19–34.
11. Wertheim MS. Fluids with highly directional attractive forces. II. Thermodynamic perturbation theory and integral equations. *J Stat Phys.* 1984;35:35–47.
12. Wertheim MS. Fluids with highly directional attractive forces. III. Multiple attraction sites. *J Stat Phys.* 1986;42:459–476.
13. Wertheim MS. Fluids with highly directional attractive forces. IV. Equilibrium polymerization. *J Stat Phys.* 1986;42:477–492.
14. Jackson G, Chapman WG, Gubbins KE. Phase equilibria of associating fluids: Spherical molecules with multiple bonding sites. *Mol Phys.* 1988;65:1–31.
15. Chapman WG, Jackson G, Gubbins KE. Phase equilibria of associating fluids: Chain molecules with multiple bonding sites. *Mol Phys.* 1988;65:1057–1079.
16. Huang SH, Radosz M. Equation of state for small, large, polydisperse, and associating molecules. *Ind Eng Chem Res.* 1990;29:2284–2294.
17. Fu YH, Sandler SI. A simplified SAFT equation of state for associating compounds and mixtures. *Ind Eng Chem Res.* 1995;34:1897–1909.
18. Chapman WG. Prediction of the thermodynamic properties of associating Lennard-Jones fluids: theory and simulation. *J Chem Phys.* 1990;93:4299–4304.
19. Müller EA, Gubbins KE. An equation of state for water from a simplified intermolecular potential. *Ind Eng Chem Res.* 1995;34:3662–3673.
20. Kraska T, Gubbins KE. Phase equilibria calculations with a modified SAFT equation of state. 1. Pure alkanes, alkanols, and water. *Ind Eng Chem Res.* 1996;35:4727–4737.
21. Kraska T, Gubbins KE. Phase equilibria calculations with a modified SAFT equation of state. 2. Binary mixtures of *n*-alkanes, 1-alkanols, and water. *Ind Eng Chem Res.* 1996;35:4738–4746.
22. Gil-Villegas A, Galindo A, Whitehead PJ, Mills SJ, Jackson G, Burgess AN. Statistical associating fluid theory for chain molecules with attractive potentials of variable range. *J Chem Phys.* 1997;106: 4168–4186.
23. Galindo A, Davies LA, Gil-Villegas A, Jackson G. The thermodynamics of mixtures and the corresponding mixing rules in the SAFT-VR approach for potentials of variable range. *Mol Phys.* 1998;93:241–252.
24. Blas FJ, Vega LF. Prediction of binary and ternary diagrams using the statistical associating fluid theory (SAFT) equation of state. *Ind Eng Chem Res.* 1998;37:660–674.
25. Blas FJ, Vega LF. Critical behavior and partial miscibility phenomena in binary mixtures of hydrocarbons by the statistical associating fluid theory. *J Chem Phys.* 1998;109:7405–7413.
26. Gross J, Sadowski G. Perturbed-Chain SAFT: An equation of state based on a perturbation theory for chain molecules. *Ind Eng Chem Res.* 2001;40:1244–1260.

27. Gross J, Sadowski G. Modeling polymer systems using the perturbed-chain statistical associating fluid theory equation of state. *Ind Eng Chem Res*. 2002;41:1084–1093.

28. von Solms N, Michelsen ML, Kontogeorgis GM. Computational and physical performance of a modified PC-SAFT equation of state for highly asymmetric and associating mixtures. *Ind Eng Chem Res*. 2003;42:1098–1105.

29. Tamouza S, Passarello JP, Tobaly P, de Hemptinne JC. Group contribution method with SAFT EOS applied to vapor liquid equilibria of various hydrocarbon series. *Fluid Phase Equilib*. 2004;222:67–76.

30. Tamouza S, Passarello JP, Tobaly P, de Hemptinne JC. Application to binary mixtures of a group contribution SAFT EOS (GC-SAFT). *Fluid Phase Equilib*. 2005;228–229:409–419.

31. Lymperiadis A, Adjiman CS, Galindo A, Jackson G. A group contribution method for associating chain molecules based on the statistical associating fluid theory (SAFT-γ). *J Chem Phys*. 2007;127:234903.

32. Lymperiadis A, Adjiman CS, Jackson G, Galindo A. A generalisation of the SAFT-γ group contribution method for groups comprising multiple spherical segments. *Fluid Phase Equilib*. 2008;274:85–104.

33. Emami FS, Vahid A, Elliott JR, Feyzi F. Group contribution prediction of vapor pressure with statistical associating fluid theory, perturbed-chain statistical associating fluid theory, and Elliott-Suresh-Donohue equations of state. *Ind Eng Chem Res*. 2008;47:8401–8411.

34. Tihic A, Kontogeorgis GM, von Solms N, Michelsen ML, Constantinou L. A predictive group-contribution simplified PC-SAFT equation of state: application to polymer systems. *Ind Eng Chem Res*. 2008;47:5092–5101.

35. Peng Y, Goff KD, dos Ramos MC, McCabe C. Developing a predictive group-contribution-based SAFT-VR equation of state. *Fluid Phase Equilib*. 2009;277:131–144.

36. Papaioannou V, Adjiman CS, Jackson G, Galindo A. Simultaneous prediction of vapour liquid and liquid liquid equilibria (VLE and LLE) of aqueous mixtures with the SAFT-γ group contribution approach. *Fluid Phase Equilib*. 2011;306:82–96.

37. Papaioannou V, Lafitte T, Avendaño C, Adjiman CS, Jackson G, Müller EA, Galindo A. Group contribution methodology based on the statistical associating fluid theory for heteronuclear molecules formed from Mie segments. *J Chem Phys*. 2014;140:054107.

38. Dufal S, Papaioannou V, Sadeqzadeh M, Pogiatzis T, Chremos A, Adjiman CS, Jackson G, Galindo A. Prediction of thermodynamic properties and phase behavior of fluids and mixtures with the SAFT-γ Mie group-contribution equation of state. *J Chem Eng Data*. 2014;59:3272–3288.

39. Fredenslund A, Jones RL, Prausnitz JM. Group-contribution estimation of activity group-contribution estimation of activity coefficients in nonideal liquid mixtures. *AIChE J*. 1975;21:1086.

40. Abrams DS, Prausnitz JM. Statistical thermodynamics of liquid mixtures: a new expression for the excess Gibbs energy of partly or completely miscible systems. *AIChE J*. 1975;21:116.

41. Müller EA, Gubbins KE. Molecular-based equations of state for associating fluids: a review of SAFT and related approaches. *Ind Eng Chem Res*. 2001;40:2193–2211.

42. Economou IG. Statistical associating fluid theory: a successful model for the calculation of thermodynamic and phase equilibrium properties of complex fluid mixtures. *Ind Eng Chem Res*. 2002;41:953–962.

43. Paricaud P, Galindo A, Jackson G. Recent advances in the use of the SAFT approach in describing electrolytes, interfaces, liquid crystals and polymers. *Fluid Phase Equilib*. 2002;194–197:87–96.

44. Tan SP, Adidharma H, Radosz M. Recent advances and applications of statistical associating fluid theory. *Ind Eng Chem Res*. 2008;47:8063–8082.

45. McCabe C, Galindo A. SAFT associating fluids and fluid mixtures. In: Goodwin ARH, Sengers JV, editors. *Applied Thermodynamics of Fluids*. London: Royal Society of Chemistry, 2010:215–279.

46. Lafitte T, Apostolakou A, Avendaño C, Galindo A, Adjiman CS, Müller EA, Jackson G. Accurate statistical associating fluid theory for chain molecules formed from Mie segments. *J Chem Phys*. 2013;139:154504.

47. Mie G. Zur kinetischen gastheorie der einatomigen körper. *Ann Phys (Leipzig)*. 1903;11:657–697.

48. Lafitte T, Bessieres D, Piñeiro MM, Daridon JL. Simultaneous estimation of phase behavior and second-derivative properties using the statistical associating fluid theory with variable range approach. *J Chem Phys*. 2006;124:024509.

49. Lafitte T, Piñeiro MM, Daridon JL, Bessieres D. A comprehensive description of chemical association effects on second derivative properties of alcohols through a SAFT-VR approach. *J Phys Chem B*. 2007;111:3447–3461.

50. Galliero G, Lafitte T, Bessieres D, Boned C. Thermodynamic properties of the Mie n - 6 fluid: a comparison between statistical associating fluid theory of variable range approach and molecular dynamics results. *J Chem Phys*. 2007;127:184506.

51. Dufal S, Lafitte T, Haslam AJ, Galindo A, Clark GNI, Vega C, Jackson G. The A in SAFT: developing the contribution of association to the Helmholtz free energy within a Wertheim TPT1 treatment of generic Mie fluids. *Mol Phys*. 2015; In press (DOI: 10.1080/00268976.2015.1029027).

52. Clark GNI, Haslam AJ, Galindo A, Jackson G. Developing optimal Wertheim-like models of water for use in statistical associating fluid theory (SAFT) and related approaches. *Mol Phys*. 2006;104:3561–3581.

53. dos Ramos MC, Docherty H, Blas FJ, Galindo A. Application of the generalised SAFT-VR approach for long-ranged square-well potentials to model the phase behaviour of real fluids. *Fluid Phase Equilib*. 2009;276:116–126.

54. Carnahan NF, Starling KE. Equation of state for nonattracting rigid spheres. *J Chem Phys*. 1969;51:635–636.

55. Barker JA, Henderson D. What is "liquid"? Understanding the states of matter. *Rev Mod Phys*. 1975;48:587–671.

56. Bett KE, Rowlinson JS, Saville G. *Thermodynamics for Chemical Engineers*. London, UK: MIT Press, 1975.

57. Levenberg K. A method for the solution of certain non-linear problems in least squares. *Q Appl Math*. 1944;2:164–168.

58. Marquardt D. An algorithm for least-squares estimation of nonlinear parameters. *J Soc Ind Appl Math*. 1963;11:431–441.

59. Sheldon TJ, Giner B, Adjiman CS, Galindo A, Jackson G, Jacquemin D, Wathelet V, Perpète EA. The derivation of size parameters for the SAFT-VR equation of state from quantum mechanical calculations, Chap. 7. In: Laso M, Perpète EA, editors. *Multiscale Modelling of Polymer Properties*. no. 22 in Computer-Aided Chemical Engineering. Amsterdam, the Netherlands: Elsevier, 2006: 143–159.

60. Linstrom P, Mallard W, editorss. *NIST Chemistry WebBook, NIST Standard Reference Database Number 69*. Gaithersburg MD: National Institute of Standards and Technology, 2013.

61. Ramrattan N, Avendaño C, Müller EA, Galindo A. A corresponding states framework for the description of the Mie family of intermolecular potentials. *Mol Phys*. In press (DOI: 10.1080/00268976.2015.1025112).

62. Camin DL, Forziati AF, Rossini FD. Physical properties of *n*-hexadecane, *n*-decylcyclopentane, *n*-decylcyclohexane, 1-hexadecene and *n*-decylbenzene. *J Phys Chem*. 1954;58:440–442.

63. Kasehgari H, Mokbel I, Viton C, Jose J. Vapor pressure of 11 alkylbenzenes in the range $10^{-3} - 280$ torr, correlation by equation of state. *Fluid Phase Equilib*. 1993;87:133–152.

64. Růžička V, Zábranský M, Růžička M, Majer V. Vapor pressures for a group of high-boiling alkylbenzenes under environmental conditions. *Thermochim Acta*. 1994;245:121–144.

65. Liessmann G, Schmidt W, Reiffarth S. Data compilation of the saechsische olefinwerke boehlen. 1995.

66. Vervekin SP. Vapour pressures and enthalpies of vaporization of a series of the linear *n*-alkyl-benzenes. *J Chem Thermodyn*. 2006;38:1111–1123.

67. London F. The general theory of molecular forces. *Trans Faraday Soc*. 1937;33:8–26.

68. Hansen JP, Weis JJ. Quantum corrections to the coexistence curve of neon near the triple point. *Phys Rev*. 1969;188:314–318.

69. Ramírez R, Herrero CP. Quantum path-integral study of the phase diagram and isotope effects of neon. *J Chem Phys*. 2008;129:204502.

70. Georgescu I, Brown SE, Mandelshtam VA. Mapping the phase diagram for neon to a quantum Lennard-Jones fluid using Gibbs ensemble simulations. *J Chem Phys*. 2013;138:134502.

71. Avendaño C, Lafitte T, Galindo A, Adjiman CS, Jackson G, Müller EA. SAFT-γ force fields for the simulation of molecular fluids: 1. A single-site coarse grained model of carbon dioxide. *J Phys Chem B*. 2011;115:11154–11169.

72. Oyewunmi OA, Taleb AI, Haslam AJ, Markides CN. An assessment of working-fluid mixtures using SAFT-VR Mie for use in organic rankine cycle systems for waste-heat recovery. *Comp Therm Sci*. 2014;6:301–316.

73. McCabe C, Jackson G. SAFT-VR modelling of the phase equilibrium of long-chain *n*-alkanes. *Phys Chem Chem Phys*. 1999;1:2057–2064.

74. Paricaud P, Galindo A, Jackson G. Modeling the cloud curves and the solubility of gases in amporphous and semicrystalline polyethylene with the SAFT-VR approach and Flory theory of crystallisation. *Ind Eng Chem Res*. 2004;43:6871–6889.

75. Kouskoumvekaki IA, von Solms N, Lindvig T, Michelsen ML, Kontogeorgis GM. Novel method for estimating pure-component parameters for polymers: application to the PC-SAFT equation of state. *Ind Eng Chem Res*. 2004;43:2830–2838.

76. Pedrosa N, Vega LF, Coutinho JAP, Marrucho I. Phase equilibria calculations of polyethylene solutions from SAFT-type equations of state. *Macromolecules*. 2006;39:4240–4246.

77. Chen SJ, Economou IG, Radosz M. Density-tuned polyolefin phase equilibria. 2. Multicomponent solutions of alternating poly(ethylene-propylene) in subcritical and supercritical olefins. Experiment and SAFT model. *Macromolecules*. 1992;25:4987–4995.

78. Chen SJ, Economou IG, Radosz M. Phase behaviour of LCST and UCST solutions of branchy copolymers: experiment and SAFT modelling. *Fluid Phase Equilib*. 1993;83:391–398.

79. Jog PK, Chapman WG, Gupta SK, Swindoll RD. Modeling of liquid–liquid-phase separation in linear low-density polyethylene–solvent systems using the statistical associating fluid theory equation of state. *Ind Eng Chem Res*. 2002;41:887–891.

80. Tumakaka F, Gross J, Sadowski G. Modeling of polymer phase equilibria using perturbed-chain SAFT. *Fluid Phase Equilib*. 2002;194–197:541–551.

81. Gross J, Spuhl O, Tumakaka F, Sadowski G. Modeling copolymer systems using the perturbed-chain SAFT equation of state. *Ind Eng Chem Res*. 2003;42:1266–1274.

82. Becker F, Buback M, Latz H, Sadowski G, Tumakaka F. Cloud-point curves of ethylene–(meth)acrylate copolymers in fluid ethylene up to high pressures and temperatures–experimental study and PC-SAFT modeling. *Fluid Phase Equilib*. 2004;215:263–282.

83. Kouskoumvekaki IA, Krooshof GJP, Michelsen ML, Kontogeorgis GM. Application of the simplified PC-SAFT equation of state to the vapor-liquid equilibria of binary and ternary mixtures of poly-amide 6 with several solvents. *Ind Eng Chem Res*. 2004;43:826–834.

84. von Solms N, Kouskoumvekaki IA, Lindvig T, Michelsen ML, Kontogeorgis GM. A novel approach to liquid-liquid equilibrium in polymer systems with application to simplified PC-SAFT. *Fluid Phase Equilib*. 2004;222:87–93.

85. Lindvig T, Michelsen ML, Kontogeorgis GM. Liquid-liquid equilibria for binary and ternary polymer solutions with PC-SAFT. *Ind Eng Chem Res*. 2004;43:1125–1132.

86. von Solms N, Michelsen ML, Kontogeorgis GM. Prediction and correlation of high-pressure gas solubility in polymers with simplified PC-SAFT. *Ind Eng Chem Res*. 2005;44:3330.

87. Haslam AJ, von Solms N, Adjiman CS, Galindo A, Jackson G, Paricaud P, Michelsen ML, Kontogeorgis GM. Predicting enhanced absorption of light gases in polyethylene using simplified PC-SAFT and SAFT-VR. *Fluid Phase Equilib*. 2006;243:74–91.

88. Pedrosa N, Vega LF, Coutinho JAP, Marrucho I. Modeling the phase equilibria of poly(ethylene glycol) binary mistures with soft-SAFT EoS. *Ind Eng Chem Res*. 2007;46:4678–4685.

89. Span R, Wagner W. A new equation of state for carbon dioxide covering the fluid region from the triple-point temperature to 1100 K at pressures up to 800 MPa. *J Phys Chem Ref Data*. 1996;25:1509–1596.

90. McCabe C, Kiselev SB. Application of crossover theory to the SAFT-VR equation of state: SAFT-VRX for pure fluids. *Ind Eng Chem Res*. 2004;43:2839–2851.

91. McCabe C, Kiselev SB. A crossover SAFT-VR equation of state for pure fluids: preliminary results for light hydrocarbons. *Fluid Phase Equilib*. 2004;219:3–9.

92. Llovell F, Pàmies JC, Vega LF. Thermodynamic properties of Lennard-Jones chain molecules: renormalization-group corrections to a modified statistical associating fluid theory. *J Chem Phys*. 2004;121:10715.

93. Forte E, Llovell F, Vega LF, Trusler JPM, Galindo A. Application of a renormalization-group treatment to the statistical associating fluid theory for potentials of variable range (SAFT-VR). *J Chem Phys*. 2011;134:154102.

94. Lafitte T, Avendaño C, Papaioannou V, Galindo A, Adjiman CS, Jackson G, Müller EA. SAFT-γ force field for the simulation of molecular fluids: 3. Coarse-grained models of benzene and hetero-group models of *n*-decylbenzene. *Mol Phys*. 2012;110:1189–1203.

95. Avendaño C, Lafitte T, Adjiman CS, Galindo A, Müller EA, Jackson G. SAFT-γ force fields for the simulation of molecular fluids: 2. Coarse-grained models of greenhouse gases, refrigerants, and long alkanes. *J Phys Chem B*. 2013;117:2717–2733.

96. Aimoli CG, Maginn EJ, Abreu CRA. Thermodynamic properties of supercritical mixtures of carbon dioxide and methane: a molecular simulation study. *J Chem Eng Data*. 2014;59:3041–3054.

97. Aimoli CG, Maginn EJ, Abreu CRA. Transport properties of carbon dioxide and methane from molecular dynamics simulations. *J Chem Phys*. 2014;141:134101.

98. Mejía A, Cartes M, Segura H, Müller EA. Use of equations of state and coarse grained simulations to complement experiments: Describing the interfacial properties of carbon dioxide + decane and carbon dioxide + eicosane mixtures. *J Chem Eng Data*. 2014;59:2928–2941.

99. Lobanova O, Avendaño C, Lafitte T, Müller EA, Jackson G. SAFT-γ force field for the simulation of molecular fluids. 4. A single-site coarse-grained model of water applicable over a wide temperature range. *Mol Phys*. In press (DOI: 10.1080/00268976.2015.1004804).

100. Müller EA, Jackson G. Force-field parameters from the SAFT-γ equation of state for use in coarse-grained molecular simulations. *Ann Rev Chem Biomolec Eng*. 2014;5:405–427.

Appendix A: A Models Based on Lennard-Jones (12-6) and the Generic Mie (λ_r-λ_a) Potentials

See Tables 1–A2.

Table A1. Intermolecular Potential Models Developed for the *n*-Alkanes Using Lennard–Jones (12-6) Potentials; * Denotes That the Highlighted Parameter is Fixed at the Indicated Value During the Parameter Estimation

Substance	Molecular Parameters					%AAD						
	m	σ / Å	λ_r	λ_a	(ε/k_B) / K	d_{liq}	u	d_{sat}	p_{sat}	c_p	T_c	ΔH_{vap}
Methane	1.0000*	3.7340	12.0*	6.0*	149.49	0.51	1.79	0.80	0.49	0.71	2.94	2.44
Ethane	1.4702	3.6905	12.0*	6.0*	199.90	0.67	4.09	0.90	0.24	1.82	0.41	1.64
Propane	1.8236	3.7810	12.0*	6.0*	219.70	0.58	9.33	0.64	0.82	2.25	2.21	1.44
Butane	2.0904	3.8965	12.0*	6.0*	238.91	0.45	4.97	0.27	0.69	2.19	1.85	1.66
Pentane	2.4361	3.9312	12.0*	6.0*	248.10	0.64	6.10	0.45	1.20	2.01	2.09	1.68
Hexane	2.7048	3.9946	12.0*	6.0*	258.62	0.75	4.72	0.50	0.43	1.35	0.68	1.71
Heptane	3.1197	3.9723	12.0*	6.0*	260.32	1.18	6.70	1.03	1.10	2.00	0.60	1.99
Octane	3.4364	3.9966	12.0*	6.0*	265.57	1.38	5.82	1.25	0.69	1.76	0.18	1.83
Nonane	3.7694	4.0093	12.0*	6.0*	269.03	1.48	8.05	1.46	0.94	1.51	0.22	1.73
Decane	4.0744	4.0309	12.0*	6.0*	272.85	1.59	7.81	1.50	0.83	0.87	3.42	1.82
Dodecane	4.7992	4.0266	12.0*	6.0*	275.65	1.77	8.15	1.74	1.09	1.39	3.02	1.95

The %AAD of the various properties calculated with the SAFT-VR Mie EOS[46] from the correlated experimental data of NIST[60] are indicated: single-phase liquid density d_{liq}; single-phase liquid speed of sound u; saturated-liquid density d_{sat}; vapor pressure p_{sat}; single-phase liquid heat capacity c_p; critical temperature T_c; enthalpy of vaporization ΔH_{vap}.

Table A2. Intermolecular Potential Models Developed for Various Hydrocarbons Using Lennard–Jones (12-6) Potentials; * Denotes That the Highlighted Parameter is Fixed at the Indicated Value During the Parameter Estimation

	Molecular Parameters					%AAD						
Substance	m	σ / Å	λ_r	λ_a	(ε/k_B) / K	d_{liq}	u	d_{sat}	p_{sat}	c_p	T_c	ΔH_{vap}
Benzene	2.2125	3.8253	12.0*	6.0*	308.59	0.41	3.05	0.18	0.41	2.34	1.95	2.35
Cyclohexane	2.2265	4.0607	12.0*	6.0*	302.32	0.67	5.33	0.25	0.26	2.30	1.69	3.24
Cyclopropane	1.6575	3.6592	12.0*	6.0*	247.79	0.75	7.82	0.40	0.14	1.84	0.63	4.72
Dimethylpropane	1.0000*	5.4536	12.0*	6.0*	363.81	3.11	6.37	2.47	11.7	9.49	9.97	8.49
Ethylene	1.4768	3.5526	12.0*	6.0*	183.63	0.44	2.87	0.75	0.68	3.55	0.89	1.97
Isobutane	2.0645	3.9267	12.0*	6.0*	229.24	0.50	11.57	0.36	1.14	1.84	1.57	1.55
Isohexane	2.7808	3.9638	12.0*	6.0*	246.75	0.99	8.68	1.07	3.66	5.11	2.24	1.42
Isopentane	2.4487	3.9236	12.0*	6.0*	239.03	0.92	7.86	1.02	4.43	3.23	0.35	1.37
Propylene	1.7920	3.6948	12.0*	6.0*	218.08	0.62	3.91	0.91	0.61	2.57	1.76	1.65
Propyne	2.0611	3.3561	12.0*	6.0*	228.75	0.23	6.36	0.53	0.45	6.28	2.14	4.69
Toluene	2.5926	3.8539	12.0*	6.0*	304.36	0.74	5.42	0.54	2.53	2.93	1.37	2.48

The %AAD of the various properties calculated with the SAFT-VR Mie EOS[46] from the correlated experimental data of NIST[60] are indicated: single-phase liquid density d_{liq}; single-phase liquid speed of sound u; saturated-liquid density d_{sat}; vapor pressure p_{sat}; single-phase liquid heat capacity c_p; critical temperature T_c; enthalpy of vaporization ΔH_{vap}.

Table A3. Intermolecular Potential Models Developed for Various Compounds Using Lennard–Jones (12-6) Potentials; * Denotes That the Highlighted Parameter is Fixed at the Indicated Value During the Parameter Estimation

	Molecular Parameters					%AAD						
Substance	m	σ / Å	λ_r	λ_a	(ε/k_B) / K	d_{liq}	u	d_{sat}	p_{sat}	c_p	T_c	ΔH_{vap}
Ar	1.0000*	3.4033	12.0*	6.0*	117.41	0.48	2.15	0.67	0.19	1.76	2.24	3.02
CO	1.2903	3.3186	12.0*	6.0*	91.515	0.40	1.66	0.62	0.21	2.92	0.55	1.63
CO_2	1.6936	3.0189	12.0*	6.0*	190.60	0.99	8.51	0.92	2.67	13.94	1.00	2.71
COS	1.5262	3.5645	12.0*	6.0*	243.24	0.44	4.11	0.77	0.93	2.61	0.82	2.18
F_2	1.2684	2.9998	12.0*	6.0*	100.44	0.40	4.50	0.62	0.11	1.46	0.26	1.51
Kr	1.0000*	3.6360	12.0*	6.0*	163.38	0.57	2.33	0.69	0.20	0.91	2.34	3.34
N_2	1.1959	3.3879	12.0*	6.0*	90.216	0.30	1.18	0.55	0.10	2.13	0.21	1.81
N_2O	1.8872	2.9405	12.0*	6.0*	181.47	0.55	9.20	0.35	0.12	2.29	1.73	3.10
Ne	1.0000*	2.8099	12.0*	6.0*	33.916	0.83	1.88	0.49	2.69	11.8	0.03	4.45
NF_3	1.6517	3.3283	12.0*	6.0*	145.16	0.37	6.02	0.54	0.32	2.40	1.05	1.92
O_2	1.0817	3.2824	12.0*	6.0*	116.45	0.77	2.50	1.04	0.24	1.65	1.68	1.51
SF_6	1.0000*	4.7035	12.0*	6.0*	262.89	2.49	7.97	1.56	7.18	12.04	8.23	9.17
SO_2	2.4368	2.8619	12.0*	6.0*	228.41	0.69	15.44	0.13	0.15	3.09	0.79	2.89
Xe	1.0000*	3.9593	12.0*	6.0*	226.80	0.59	2.81	0.78	0.22	1.28	2.72	3.37

The %AAD of the various properties calculated with the SAFT-VR Mie EOS[46] from the correlated experimental data of NIST[60] are indicated: single-phase liquid density d_{liq}; single-phase liquid speed of sound u; saturated-liquid density d_{sat}; vapor pressure p_{sat}; single-phase liquid heat capacity c_p; critical temperature T_c; enthalpy of vaporization ΔH_{vap}.

Table A4. Intermolecular Potential Models Developed for the *n*-Alkanes Using Generic Mie (λ_r-λ_a) Potentials; * Denotes That the Highlighted Parameter is Fixed at the Indicated Value During the Parameter Estimation

	Molecular Parameters					%AAD						
Substance	m	σ / Å	λ_r	λ_a	(ε/k_B) / K	d_{liq}	u	d_{sat}	p_{sat}	c_p	T_c	ΔH_{vap}
Methane	1.0000*	3.7710	19.650	4.4487	113.05	0.50	3.77	0.26	0.25	3.77	1.80	2.55
Ethane	1.8073	3.4133	8.3898	6.7055	158.31	0.57	6.67	0.39	0.41	2.61	2.43	1.47
Propane	1.7610	3.8329	12.954	5.8542	226.30	0.58	9.57	0.69	0.76	2.25	1.32	1.45
Butane	1.6772	4.2495	15.513	5.9910	306.65	0.34	2.43	0.58	0.09	0.93	1.82	1.46
Pentane	1.9068	4.3309	15.075	6.1999	333.12	0.21	2.50	0.34	0.13	0.96	2.44	1.39
Hexane	2.2747	4.2817	14.545	6.0880	320.91	0.28	1.97	0.30	0.14	0.88	2.52	1.69
Heptane	2.3879	4.4257	13.439	6.8824	377.36	0.26	2.15	0.14	0.09	0.93	3.36	1.73
Octane	2.5913	4.4882	13.061	7.1807	399.20	0.38	1.39	0.19	0.09	1.00	3.53	1.71
Nonane	2.7930	4.5379	13.123	7.2319	412.06	0.24	1.71	0.14	0.06	0.89	3.46	1.67
Decane	3.0670	4.5389	13.311	7.1398	412.68	0.35	2.17	0.15	0.08	0.95	3.76	1.95
Dodecane	3.2923	4.7212	15.678	6.8784	454.37	0.40	1.65	0.22	0.24	1.13	3.49	2.07

The %AAD of the various properties calculated with the SAFT-VR Mie EOS[46] from the correlated experimental data of NIST[60] are indicated: single-phase liquid density d_{liq}; single-phase liquid speed of sound u; saturated-liquid density d_{sat}; vapor pressure p_{sat}; single-phase liquid heat capacity c_p; critical temperature T_c; enthalpy of vaporization ΔH_{vap}.

Table A5. Intermolecular Potential Models Developed for Various Hydrocarbons Using Generic Mie (λ_r-λ_a) Potentials; * Denotes That the Highlighted Parameter is Fixed at the Indicated Value During the Parameter Estimation

| Substance | Molecular Parameters | | | | | %AAD | | | | | | |
	m	σ / Å	λ_r	λ_a	(ε/k_B) / K	d_{liq}	u	d_{sat}	p_{sat}	c_p	T_c	ΔH_{vap}
Benzene	1.9897	3.9905	16.590	5.3795	329.67	0.47	1.87	0.23	0.31	2.40	1.21	2.28
Cyclohexane	1.8592	4.3660	18.447	5.3693	349.99	0.37	2.43	0.17	0.25	2.32	2.06	3.26
Cyclopropane	1.0290	4.4323	19.327	6.7466	445.93	1.27	13.58	0.29	0.26	4.71	3.37	5.86
Dimethylpropane	1.0000*	5.6596	50.000	5.2201	462.53	1.09	7.07	0.27	0.41	1.79	2.33	3.50
Ethylene	1.2428	3.7865	10.160	7.8693	242.67	0.46	2.23	0.62	0.23	1.97	0.12	1.44
Isobutane	1.6240	4.3159	17.164	5.7007	290.71	0.40	7.40	0.62	0.33	1.68	1.96	1.48
Isohexane	2.2025	4.3415	16.406	5.7892	313.38	0.53	4.08	0.42	1.47	4.68	3.13	1.49
Isopentane	1.8246	4.3920	14.632	6.2913	332.07	0.29	3.07	0.36	0.29	0.94	2.57	1.18
Propylene	1.8798	3.6285	11.843	5.8588	204.23	0.57	4.10	0.67	0.74	2.60	1.54	1.58
Propyne	2.4395	3.1374	8.5420	6.7752	190.07	0.32	6.98	0.15	0.52	6.81	0.34	4.51
Toluene	1.8278	4.4263	15.327	6.5140	461.73	0.27	2.09	0.44	0.11	1.28	2.04	1.82

The %AAD of the various properties calculated with the SAFT-VR Mie EOS[46] from the correlated experimental data of NIST[60] are indicated: single-phase liquid density d_{liq}; single-phase liquid speed of sound u; saturated-liquid density d_{sat}; vapor pressure p_{sat}; single-phase liquid heat capacity c_p; critical temperature T_c; enthalpy of vaporization ΔH_{vap}.

Table A6. Intermolecular Potential Models Developed for Various Compounds Using Generic Mie (λ_r-λ_a) Potentials; * Denotes That the Highlighted Parameter is Fixed at the Indicated Value During the Parameter Estimation

| Substance | Molecular Parameters | | | | | %AAD | | | | | | |
	m	σ / Å	λ_r	λ_a	(ε/k_B) / K	d_{liq}	u	d_{sat}	p_{sat}	c_p	T_c	ΔH_{vap}
Ar	1.0000*	3.4273	17.713	4.6312	93.381	0.47	4.03	0.20	0.17	4.99	1.64	2.93
CO	1.5528	3.0950	9.7981	5.9827	72.21	0.31	2.35	0.15	0.08	2.65	1.61	1.27
CO_2	1.6936	3.0490	26.408	5.055	207.89	1.30	18.80	0.06	0.27	4.99	0.35	3.04
$CO_2{}^a$	1.5000	3.1916	27.557	5.1646	231.88	0.53	2.40	0.15	0.07	2.64	1.84	3.28
COS	1.2607	3.8273	10.269	7.8823	327.62	0.59	3.57	0.70	0.21	1.82	0.26	1.52
F_2	1.5397	2.7905	9.2354	6.2446	79.713	0.36	6.16	0.25	0.02	1.92	1.74	1.23
Kr	1.0000*	3.6667	18.219	4.5072	123.77	0.43	4.24	0.20	0.16	4.42	1.68	3.16
N_2	1.4836	3.1243	8.2863	6.6863	70.256	0.59	3.54	0.14	0.05	2.45	1.84	1.39
N_2O	2.0204	2.8616	11.442	5.8897	165.83	0.53	7.62	0.09	0.04	2.05	2.09	3.00
Ne	1.0000*	2.7991	8.8941	6.4568	30.626	0.44	6.90	0.04	0.43	4.31	1.73	2.02
NF_3	1.5434	3.4171	13.456	5.8529	155.22	0.39	5.38	0.67	0.25	2.22	1.04	1.98
O_2	1.4595	2.9427	8.0813	6.4062	80.36	0.57	5.47	0.38	0.22	2.76	2.30	1.03
SF_6	1.0000*	4.8811	50.000	5.4185	358.00	1.05	6.66	0.08	0.35	5.81	2.16	4.33
SO_2	2.6207	2.7813	9.7327	6.5569	213.44	0.63	13.23	0.10	0.14	3.13	0.55	2.90
Xe	1.0000*	3.9941	18.910	4.4840	172.29	0.52	5.85	0.20	0.14	5.07	1.85	3.41

The %AAD of the various properties calculated with the SAFT-VR Mie EOS[46] from the correlated experimental data of NIST[60] are indicated: single-phase liquid density d_{liq}; single-phase liquid speed of sound u; saturated-liquid density d_{sat}; vapor pressure p_{sat}; single-phase liquid heat capacity c_p; critical temperature T_c; enthalpy of vaporization ΔH_{vap}.
^aDenotes models taken from Ref. 46.